A DYNAMIC CIRCUIT MECHANISM FOR SOCIAL BOND FORMATION IN FEMALE PRAIRIE VOLES

A Dissertation
Presented to
The Academic Faculty

by

Elizabeth A. Amadei

In Partial Fulfillment
of the Requirements for the Degree
Doctor of Philosophy in the
Wallace H. Coulter Department of Biomedical Engineering

Georgia Institute of Technology
Emory University

May 2017

A DYNAMIC CIRCUIT MECHANISM FOR SOCIAL BOND FORMATION IN FEMALE PRAIRIE VOLES

Approved by:

Dr. Robert Liu, Advisor
College, Department of Biology
Emory University

Dr. Joseph Manns
College, Department of Psychology
Emory University

Dr. Larry Young, Co-advisor
School of Medicine, Department of Psychiatry
Emory University

Dr. Samuel Sober
College, Department of Biology
Emory University

Dr. Robert Butera
School of Biomedical Engineering
Georgia Institute of Technology

Date Approved: January 26, 2017

To Mom, Dad, Alex and Fabian for your love and support.

ACKNOWLEDGEMENTS

I would like to thank the many people who contributed to this work. These include my advisors, Dr. Robert Liu and Dr. Larry Young, and thesis committee members, Dr. Joseph Manns, Dr. Samuel Sober and Dr. Robert Butera. These individuals have provided extensive mentoring and support over the years, and I am deeply grateful for the time and energy they have invested into my professional development. I would also like to thank the co-authors of the manuscript encompassing my work. Each person made important intellectual and technical contributions that helped me to bring this manuscript to fruition. In addition to my advisors, these co-authors are Dr. Zachary Johnson, Yong Jun (Jim) Kwon, Aaron Shpiner, Varun Saravanan, Wittney Mays, Dr. Steven Ryan, Dr. Hasse Walum and Dr. Donald Rainnie.

I further thank Dr. Hans-Peter Lipp for Neurologgers; Dr. Frank Lin for initial testing of Neurologgers; Dr. Gordon Berman for methodological feedback and fruitful discussions; Gerald Wong for behavioral scoring; Mengqi Zhang, Rasika Tangutoori and Rachel Stanford for assistance with implant design and construction; the Liu, Young and Rainnie laboratories for training, feedback and helpful discussions; Lorra Matthews and the Yerkes animal care and veterinary staff for vole husbandry and care; Garrett Feldpausch for custom cage design and machining; and Dr. Jamie LaPrairie and Li-Ling Shen for their assistance.

Finally, I could not have done this work without the love and support of my family – Robin, Bernard and Alex – and my boyfriend, Fabian. Thank you for always being there to provide affection and encouragement.

This work was funded by an Emory Neuroscience Initiative grant (R.L., L.Y.), NIMH R21MH97187 (R.L.), NIMH P50MH100023 (L.Y., R.L.) and NINDS 1T90DA032466 (V.S.).

TABLE OF CONTENTS

LIST OF FIGURES

LIST OF SYMBOLS AND ABBREVIATIONS

α	significance level
Δ	change
AAV	adeno-associated virus
AC	anterior cingulate cortex
aCSF	artificial cerebrospinal fluid
A/P	anterior-posterior
B	baseline
BLA	basolateral amygdala
BNST	bed nucleus of the stria terminalis
cc	corpus callosum
ChR2	Channelrhodopsin-2
CSDS	chronic social defeat stress
D2R	dopamine 2 receptors
DA	dopamine
DAPI	4’,6-Diamidino-2-Phenylindole, Dihydrochloride
DNQX	6,7-dinitroquinoxaline-2,3-dione
EPSC	excitatory post-synaptic current
EPSP	excitatory post-synaptic potential
EYFP	enhanced yellow fluorescent protein
FSI	fast-spiking interneuron
Hud	huddling
Hyp	hypothalamus
IEG	immediate early gene

IL	infralimbic cortex
LFP	local field potential
M	mating
M+	after mating
M-	before mating
MI	Modulation Index
M/L	medial-lateral
MO	medial orbital cortex
mPFC	medial prefrontal cortex
MSN	medium spiny neuron
NAcc	nucleus accumbens
NC	non-coded
NGS	normal goat serum
NHud	nonhuddling
OT	oxytocin
OTR	oxytocin receptors
P	partner
P	P-value
P_{un}	P-value (uncorrected)
PBS	phosphate buffered saline
PBST	phosphate buffered saline triton
PFA	paraformaldehyde
Picro	picrotoxin
PL	prelimbic cortex
PPT	partner preference test
R^2	square of Pearson correlation coefficient

S	stranger
SG	self-grooming
SG+	after self-grooming
SG-	before self-grooming
shRNA	short hairpin RNA
SHy	septohypothalamic nucleus
T	multitaper segment duration
TTX	tetrodotoxin
VTA	ventral tegmental area
W	spectral concentration bandwidth

SUMMARY

Adult pair bonding involves dramatic changes in the perception and valuation of another individual (Hazan and Shaver, 1987; Zayas et al., 2015). One key change is that partners come to reliably activate the brain's reward system (Aragona et al., 2006; Bartels and Zeki, 2000; Johnson et al., 2016; Ross et al., 2009b; Young et al., 2001), though the precise neural mechanisms by which partners become rewarding during sociosexual interactions leading to a bond remain unclear. Using a prairie vole model of social bonding (Young and Wang, 2004), I show how a functional circuit from medial prefrontal cortex (mPFC) to nucleus accumbens (NAcc) is dynamically modulated to enhance females' affiliative behavior towards a partner. Individual variation in the strength of this functional connectivity, particularly after the first mating encounter, predicts how quickly animals begin affiliative huddling with their partner. Rhythmically activating this circuit in a social context without mating biases later preference towards a partner, indicating that this circuit's activity is not just correlated with how quickly animals become affiliative but causally accelerates it. These results provide the first dynamic view of corticostriatal processes involved in bond formation, revealing how social interactions recruit reward systems to drive changes in affiliative behavior.

CHAPTER 1

INTRODUCTION

The ability to form social attachments throughout one's lifespan is crucial for well-being and mental health (NAMHC, 2004). Such attachments include adult pair bonding, for which the brain areas activated during pair bond expression have been examined using functional magnetic resonance imaging studies in humans (Acevedo et al., 2011; Bartels and Zeki, 2000). However, the precise neural mechanisms of pair bond formation are technically challenging to study in humans, motivating the use of animal models. This thesis takes advantage of the prairie vole (*Microtus ochrogaster*), a canonical rodent model of social bonding (Johnson and Young, 2015; Young and Wang, 2004). In the Introduction sections below, I describe the laboratory preparation and previous work examining neurochemical mechanisms of vole bonding within the mesocorticolimbic reward system. I focus on two anatomically-connected brain areas, the mPFC and NAcc (Christie et al., 1987; Gorelova and Yang, 1996; Ross et al., 2009a), for which I detail unanswered questions and lay out the objectives of this thesis.

1.1 Prairie Vole Model of Social Bonding

The prairie vole is a socially monogamous rodent that forms life-long bonds with partners (Young and Wang, 2004). The first evidence for prairie vole pair bonding came from live-trap field studies of prairie voles and meadow voles (*Microtus pennsylvanicus*), a closely-related, but polygamous, vole species. Compared to meadow voles, prairie voles were more likely to be captured in male-female pairs as well as re-captured in the same pairs over time (Getz et al., 1981). In preliminary laboratory studies, wild-derived female prairie voles separately exposed to their breeding partner and a novel male showed more mating and less aggression towards the partner (Getz et al., 1981), consistent with field observations and motivating the development of laboratory

preparations for pair bond formation and expression. Pair bond formation ("cohabitation", Figure 1.1, left) consists of pairing two opposite-sex adults typically for 6 to 48 hours (Williams et al., 1992). A subject's bond with its partner is then assessed using a partner preference test (PPT, Figure 1.1, right), in which the partner from cohabitation is tethered to one side of a three-chambered arena, while a stranger of same sex to the partner is tethered to the other side (Ahern et al., 2009). The relative amount of time that the freely-moving subject spends in motionless physical contact ("huddling") with its partner versus the stranger ("partner preference") is used as an index of bond formation. Prairie voles form robust partner preferences, whereas the closely-related, but polygamous, montane voles (*Microtus montanus*) do not (Insel and Hulihan, 1995).

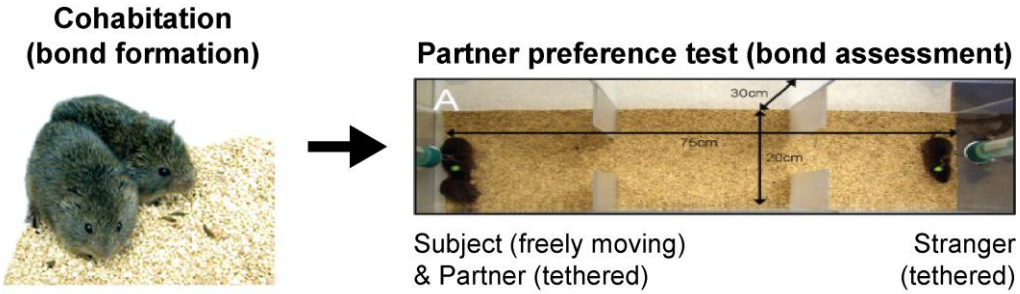

Figure 1.1 | Laboratory preparations for vole bond formation and assessment. Extended male-female pairing (**left**) can produce a social bond that is assessed using the PPT (**right**). During the PPT, the subject chooses to huddle with the partner from cohabitation versus a stranger, and the relative time spent with each individual is measured as an index of the bond. Images adapted from Lim et al. (2004) and Ahern et al. (2009).

Based on previous work in postpartum females demonstrating mating preference for their breeding partner and aggression toward novel males (Getz et al., 1981), Williams et al. (1992) tested whether mating facilitates bond formation in females. They estrogen-primed a group of ovariectomized females to induce sexual receptivity. A second group was left untreated. Both groups were cohabitated with males for 6 hours and then tested in a PPT. During the cohabitation, a subset of estrogen-primed females

failed to mate and thus were classified as a non-mating, estrogen-primed group. When comparing the PPT results across groups, only females that mated within cohabitation developed a partner preference, whereas non-mating, estrogen-primed females and un-treated females did not. Williams et al. (1992) also showed that 24 hours of cohabitation is sufficient for partner preference formation even in the absence of mating, indicating that mating accelerates bond formation.

1.2 Neurochemistry of Prairie Vole Social Bonding

The availability of closely-related species with different social strategies led to an important study by Insel and Shapiro (1992) measuring the distribution of brain oxytocin receptors (OTR) in prairie and montane voles. They found significant differences in OTR levels in several brain areas, including elevated OTR in the mPFC and NAcc of prairie voles. Their findings led to the hypothesis that oxytocin (OT), as well as other neurochemicals known to be released during social interactions (e.g. dopamine (DA) (Damsma et al., 1992)), act within these brain areas to facilitate bond formation (Figure 1.2). In this Introduction, I will summarize key studies that measure neurochemical release during social interactions leading to a bond, inhibit neurochemical action to disrupt bond formation, enhance neurochemical action to accelerate bond formation, and examine neurochemicals' influence on brain networks.

1.2.1 Measurement of Neurochemical Release During Social Interactions

Given the role of mating in accelerating vole bond formation (Williams et al., 1992) and the finding that vaginocervical stimulation induces central OT release in sheep (Kendrick et al., 1986a) (see below), Ross et al. (2009a) tested whether mating releases OT into the NAcc of female prairie voles. They measured OT dialysates from the NAcc of female voles cohabitating with a male. To isolate the effect of mating, females underwent a "restricted exposure" phase, in which the male was placed in the same cage as the female but separated by a wire mesh to prevent mating, and then a

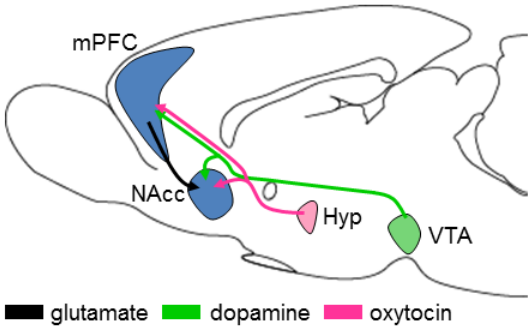

Figure 1.2 | Proposed neural circuits of vole bond formation. mPFC and NAcc receive OT and DA projections from the hypothalamus (Hyp) and ventral tegmental area (VTA), respectively. mPFC projects glutamatergically to the NAcc. Figure adapted from Young and Wang (2004) and McGraw and Young (2010).

"free exposure" phase allowing mating. Females were categorized by whether they mated during free exposure. Specifically in the mating group, the percentage of females with detectable (above threshold) dialysate readings significantly increased from the restricted- to free-exposure phases, suggesting mating releases OT in NAcc.

Gingrich et al. (2000) measured NAcc DA dialysates in mating and non-mating female voles freely-exposed to a male. They found a significant increase in DA specifically in mating females within the first 15 minutes of cohabitation (compared to a 15-min baseline period before male exposure), suggesting that mating releases DA in NAcc.

Central OT and DA release during mating or vaginocervical stimulation has been found in other species as well. For example, using microdialysis in male and female rats, Damsma et al. (1992) and Pfaus et al. (1995) found a significant increase in NAcc DA during mating compared to a baseline time point. Waldherr and Neumann (2007) and Nyuyki et al. (2011) found a significant increase in OT at the paraventricular nucleus of the hypothalamus, a key site of OT production (Kendrick, 2000), in male rats and female rats able to pace their mating behavior. Sampling cerebrospinal fluid from the lateral ventricles of cycling female sheep, Kendrick et al. (1986b) found that vaginocervical

stimulation significantly elevated central OT levels. These results indicate that the mating-induced release of OT and DA is not itself specific to prairie voles. However, parallel studies in voles inhibited or enhanced neurochemical action in the NAcc and other brain areas to determine how neurochemicals specifically act to facilitate vole bond formation. These studies are summarized below.

1.2.2 Inhibition of Brain Neurochemical Systems

The first inhibition studies infused neurochemical receptor antagonists centrally or systemically to block neurochemicals' action during vole bonding. Blocking OTR centrally or DA 2 receptors (D2R) systemically disrupted bond formation (Insel and Hulihan, 1995; Wang et al., 1999). Subsequent site-specific antagonist studies implicated mPFC and NAcc as key sites of neurochemical action. Blocking OTR in either mPFC or NAcc or D2R in NAcc disrupted bond formation in mating females (Gingrich et al., 2000; Young et al., 2001). Blocking central OTR and NAcc D2R also disrupted bond formation in mating males (Aragona et al., 2006; Johnson et al., 2016), thus extending results to both sexes.

Keebaugh et al. (2015) knocked down OTR expression in NAcc to further test the necessity of OT's NAcc action for bond formation. Juvenile females were injected with an adeno-associated virus (AAV) carrying a short hairpin RNA (shRNA) that degraded OTR mRNA, thus reducing OTR expression. In adulthood, treated females were cohabitated with a partner for 24 hours with mating. In contrast to animals injected with a control virus, treated animals failed to show a partner preference, thereby further implicating NAcc OTR in bond formation. However, how OTR activation affects neural activity in NAcc remains an open question.

1.2.3 Enhancement of Brain Neurochemical Systems

While pharmacological inhibition and receptor knock down studies demonstrated the necessity of OT and DA for vole bond formation, other pharmacological and genetic

studies enhanced OT and DA function to test these neurochemicals' sufficiency. For example, Williams et al. (1994) and Insel and Hulihan (1995) found that central OT infusion (compared to vehicle, artificial cerebrospinal fluid (aCSF)) accelerated bond formation in females even in the absence of mating. Cho et al. (1999) performed central OT infusion in both non-mating males and females and found a similar acceleration effect in both sexes. To augment OT action within the NAcc specifically, Ross et al. (2009b) overexpressed NAcc OTR in females by injecting an AAV carrying the OTR gene. Compared to a sham-surgery control group lacking the AAV, treated animals more quickly developed a partner preference when tested at multiple time points. Also within the NAcc, infusion of the D2R agonist quinpirole accelerated bond formation in both non-mating females (Gingrich et al., 2000) and males (Aragona et al., 2006).

1.2.4 Neurochemical Influence on Brain Networks

The neurochemical measurement and manipulation studies described above established the importance of individual brain areas for social bond formation. More recently, Johnson et al. (2016) and Johnson et al. (2017) investigated how OT modulates immediate early gene (IEG) expression across brain areas. Males were infused with OTA or aCSF vehicle either centrally or within the NAcc and then cohabitated with a female with mating. Following cohabitation, the males' brains were removed and expression of the IEG protein Fos, a measure of neuronal activation, quantified in multiple areas implicated in prairie vole bonding and social behavior (e.g. mPFC, NAcc, medial and basolateral amygdala (BLA)). While OTA and aCSF animals showed comparable amounts of mating and investigative behaviors as well as Fos expression in individual brain areas, the correlation between brain areas' Fos expression was disrupted in OTA animals, suggesting that OT enhances coordinated IEG expression within a network of brain areas.

Neurochemical measurement, inhibition and enhancement studies have been critical for implicating mPFC and NAcc in bond formation. Also, the recent IEG studies have raised the possibility that mPFC and NAcc become activated together and as part of a broader network as animals socially interact. However, these findings provide only a static picture of mPFC and NAcc involvement in bond formation. How these brain areas are dynamically activated during social interaction leading to a bond has been unknown. In this thesis, I address this gap by recording and manipulating dynamic neural activity within the mPFC and NAcc of socially interacting female voles. As background to the formal objectives of this thesis (Section 1.5 below), I will next briefly summarize mPFC and NAcc anatomy and previous work on functional connectivity.

1.3 mPFC and NAcc Anatomy

The mPFC and NAcc are part of the mesocorticolimbic system, composed of the VTA, a key locus of DA neurons, and its projection sites (Swanson, 1982; van Huijstee and Mansvelder, 2015). These projection sites can be classified into a limbic areas including the NAcc, amygdala, hippocampus and cortical areas including the mPFC and orbitofrontal cortex (Hearing et al., 2012). This system has been implicated in natural reward and reinforcement (Hernandez and Hoebel, 1988; Schultz, 2006), and is also recruited by drugs of abuse to elicit pathological drug-seeking behaviors (Adinoff, 2004; Bossert et al., 2012).

The mPFC has been implicated in behavioral flexibility (Ragozzino et al., 1999), attention (Kahn et al., 2012) and decision making (Walton et al., 2002). The rodent mPFC consists of four cortical sub-regions (from dorsal to ventral): medial agranular, anterior cingulate (AC), prelimbic (PL) and infralimbic (IL) (Hoover and Vertes, 2007). These sub-regions are distinguished by their cytoarchitecture (e.g. lamination, cell density) (van Eden and Uylings, 1985) and connectivity (Hoover and Vertes, 2007). For example, dorsal mPFC (medial agranular, dorsal AC) is more strongly innervated by

sensorimotor cortical areas, whereas ventral mPFC (PL, IL) is more strongly innervated by limbic areas (e.g. amygdala, limbic cortical areas) (Hoover and Vertes, 2007). Dorsal and ventral mPFC also differ in their projection targets. For example, within the NAcc, which is divided into core and shell sub-regions (see below), dorsal mPFC more strongly innervates the core, while ventral (IL) mPFC more strongly innervates the shell, all glutamatergically (Brog et al., 1993; Christie et al., 1987). Within the mPFC, as in other cortical areas, a balance of excitation and inhibition exists between excitatory pyramidal neurons and inhibitory interneurons (Yizhar et al., 2011).

The NAcc plays a key role in selecting motivated behavioral responses to environmental stimuli (Floresco, 2015; Ghods-Sharifi and Floresco, 2010; Nicola, 2007). The NAcc consists of two primary sub-regions (from medial to lateral): shell and core. The NAcc sub-regions differ in their cell morphology, histochemistry and connectivity (Heimer et al., 1991; Meredith et al., 1992). For example, while both core and shell project to the ventral pallidum, a major limbic output structure (Smith et al., 2009), the shell shows a distinguishing projection to the extended amygdala (Heimer et al., 1991). The NAcc is primarily an inhibitory structure, in which 90-95% of neurons are GABAergic medium spiny neurons (MSNs) (Nicola et al., 2000). The remaining 5-10% are interneurons including fast-spiking parvalbumin (FSIs), slow-firing cholinergic and burst-firing somatostatin/nitric oxide (Nicola et al., 2000; Tepper et al., 2008). MSNs project intrinsically to each other (Taverna et al., 2004), as well as externally (Chang and Kitai, 1985), and receive projections from local interneurons (Taverna et al., 2007). The following section will focus on the functional role of mPFC glutamatergic projections to the NAcc (mPFC-NAcc “circuit”).

1.4 mPFC-NAcc Functional Connectivity

Functional connectivity will be treated here as general term to encompass the following three ways of assaying activation of the mPFC-NAcc circuit and its role in

behavior: 1) correlation in electrophysiological activity between brain areas, 2) asymmetrical lesions of brain areas across hemispheres to disconnect the projection and 3) optogenetic stimulation of mPFC afferents in the NAcc. This section will focus on previous work applying these methods to examine the mPFC-NAcc circuit's function in motivated behavior and learning.

Gruber et al. (2009a) measured spiking and local field potential (LFP) activity from the mPFC and NAcc of rats during lever-pressing for a sucrose reward. LFPs are an integrated signal of population activity, thought to reflect synchronized synaptic inputs, spike afterpotentials, and subthreshold membrane fluctuations of neurons near the electrode tip (Berens et al., 2008). Compared to an active control behavior of exploration within the experiment cage, lever pressing enhanced the cross-correlation in mPFC-NAcc spiking as well as the cross-spectral density of mPFC and NAcc LFPs at low frequencies (delta; 1-4 Hz), two measures of connectivity. Thus, motivated reward-seeking behavior recruited the mPFC-NAcc circuit, particularly at low frequencies.

Block et al. (2007) manipulated mPFC-NAcc connectivity to examine its role in attentional set shifting, a measure of behavioral flexibility in which the stimulus associated with rewarded behaviors changes over the course of the experiment. In this study, rats first learned to use a spatial cue within a maze to choose the path leading to reward ("response strategy"). The task design was then updated such that a visual cue now predicted the rewarded path whereas the spatial cue was non-informative ("visual cue-based strategy"). To test the mPFC-NAcc circuit's role in shifting behavioral strategies, Block et al. disconnected the mPFC-NAcc circuit by asymmetrically lesioning mPFC and NAcc across brain hemispheres. Compared to a saline-injected control group, mPFC-NAcc disconnected animals acquired the response strategy normally, but were selectively disrupted in their switch to the visual cue-based strategy, as indicated by a significantly greater number of perseverative errors and trials needed to reach a

performance threshold on the visual cue-based task. Therefore, mPFC-NAcc connectivity was necessary for flexible adjustments in behavior on this set shifting task.

To test the sufficiency of mPFC-NAcc connectivity in modifying motivated behaviors, Britt et al. (2012) and Bagot et al. (2015) optogenetically stimulated this circuit in conditioned place preference and chronic social defeat stress (CSDS) assays, respectively, as described below. Both studies used low-frequency stimulation (6 Hz or 4 Hz, respectively; no other stimulation frequencies were reported).

In the Britt et al. study, stimulation was delivered whenever an animal entered one side of the testing arena. Animals' preference for that location was measured during the stimulation session (repeated twice on the two following days) as well as prior to and following the stimulation sessions (pre- and probe-tests). mPFC-NAcc stimulation enhanced preference for the stimulation location, indicated by a significant effect of experiment session on preference for the stimulation-paired location.

In the Bagot et al. study, animals underwent a CSDS paradigm in which they were repeatedly exposed to an aggressor mouse. They were then implanted with optical fibers and the mPFC-NAcc circuit stimulated during exposure to a novel stimulus mouse, which normally elicits social avoidance. Compared to control animals without optical stimulation, stimulated animals spent more time in social proximity to the stimulus mouse and less time in the cage corners, indicating that low-frequency mPFC-NAcc stimulation reduced social avoidance and enhanced social investigation. Therefore, both Britt et al. (2012) and Bagot et al. (2015) demonstrated that low-frequency mPFC-NAcc activation can modify motivated behaviors.

These four studies demonstrate that motivated behaviors both recruit and are influenced by mPFC-NAcc circuit activation. In particular, low-frequency activity appears to predominate during reward seeking and help to shift animals to a new behavioral response to a given stimulus in both non-social and social contexts. This motivates

asking whether mPFC-NAcc functional connectivity could also play a role in vole pair bonding, in which animals become increasingly affiliative towards a partner over the course of cohabitation. I investigate this question in this thesis, with the central hypothesis that mPFC-NAcc functional connectivity during bond formation helps to switch animals to express affiliative behavior towards a partner.

1.5 Objectives and Summary

In this thesis, I investigate the role of mPFC-NAcc functional connectivity in vole pair bonding by recording and manipulating this circuit during natural social interactions leading to a bond. The specific objectives are to:

1) Develop experimental preparations for LFP recording and optogenetic manipulation in freely-behaving, socially-interacting female voles.

2) Measure natural behaviors occurring during cohabitation, including mating, a behavior that accelerates bond formation, and huddling, a measure of bond expression (see above). Characterize the emergence of huddling behavior over the course of cohabitation.

3) Measure functional connectivity between mPFC and NAcc over the course of cohabitation and relate this connectivity to the emergence of huddling behavior.

4) Optogenetically stimulate this circuit to causally test its role in facilitating bond formation.

I show that low-frequency coherence, one measure of functional connectivity, between mPFC and NAcc is enhanced during mating. To assess how this low-frequency connectivity modulates local activity in individual brain areas, I assess cross-frequency interactions between brain areas. I find that the phase of low-frequency mPFC oscillations modulates the amplitude of NAcc high (gamma)-frequency oscillations, a measure of local network activation (Buzsáki and Wang, 2012), suggesting that mPFC modulates local activity in NAcc. The strength of this modulation varies across

individuals and predicts how quickly animals begin affiliative huddling with their partner. To test whether mPFC-NAcc circuit activation causally facilitates bond formation, I optogenetically activate this circuit in a social context without mating and find that this activation biases later preference towards a partner. These results are consistent with the central hypothesis that mPFC-NAcc functional connectivity during bond formation helps to switch animals to express affiliative behavior towards a partner.

CHAPTER 2

DYNAMIC CORTICOSTRIATAL ACTIVITY BIASES SOCIAL BONDING IN MONOGAMOUS FEMALE PRAIRIE VOLES[1]

2.1 Introduction

The formation of socially monogamous relationships, or pair bonds, is a complex phenomenon occurring in less than 5% of mammalian species (Kleiman, 1977). In the monogamous prairie vole, neurochemicals (e.g. OT, DA) (Young and Wang, 2004) act in two anatomically-connected (Christie et al., 1987; Ross et al., 2009a) corticostriatal areas, the mPFC and NAcc, to establish a selective preference towards a partner (Aragona et al., 2006; Young and Wang, 2004). Individual variation in neurochemical receptors within this circuit explains differences in affiliative behavior (Aragona et al., 2006; Ross et al., 2009b). However, little is known about how mPFC and NAcc are dynamically activated during sociosexual interactions. mPFC-NAcc communication is more generally implicated in an animal's ability to effectively coordinate its behavior to obtain rewards (Floresco, 2015; Nicola, 2007), including gaining new behavioral strategies (Block et al., 2007). I therefore hypothesized that mPFC-NAcc functional connectivity helps to switch animals to express affiliative behavior towards a partner.

2.2 Results

To examine the neural and behavioral specificity of this hypothesis, I developed an electrophysiological recording paradigm for freely-moving females during extended sociosexual interactions with a male (Figure 2.1a-c). Electrodes were chronically implanted (Figure 2.2a-c) in the mPFC and NAcc (hit animals) or an off-target area

[1] Adapted from E.A. Amadei*, Z.V. Johnson*, Y.-J. Kwon, A.C. Shpiner, V. Saravanan, W.D. Mays, S.J. Ryan, H. Walum, D.G. Rainnie, L.J. Young and R.C. Liu, Dynamic corticostriatal activity biases social bonding in monogamous prairie voles, **Nature**. In revision.

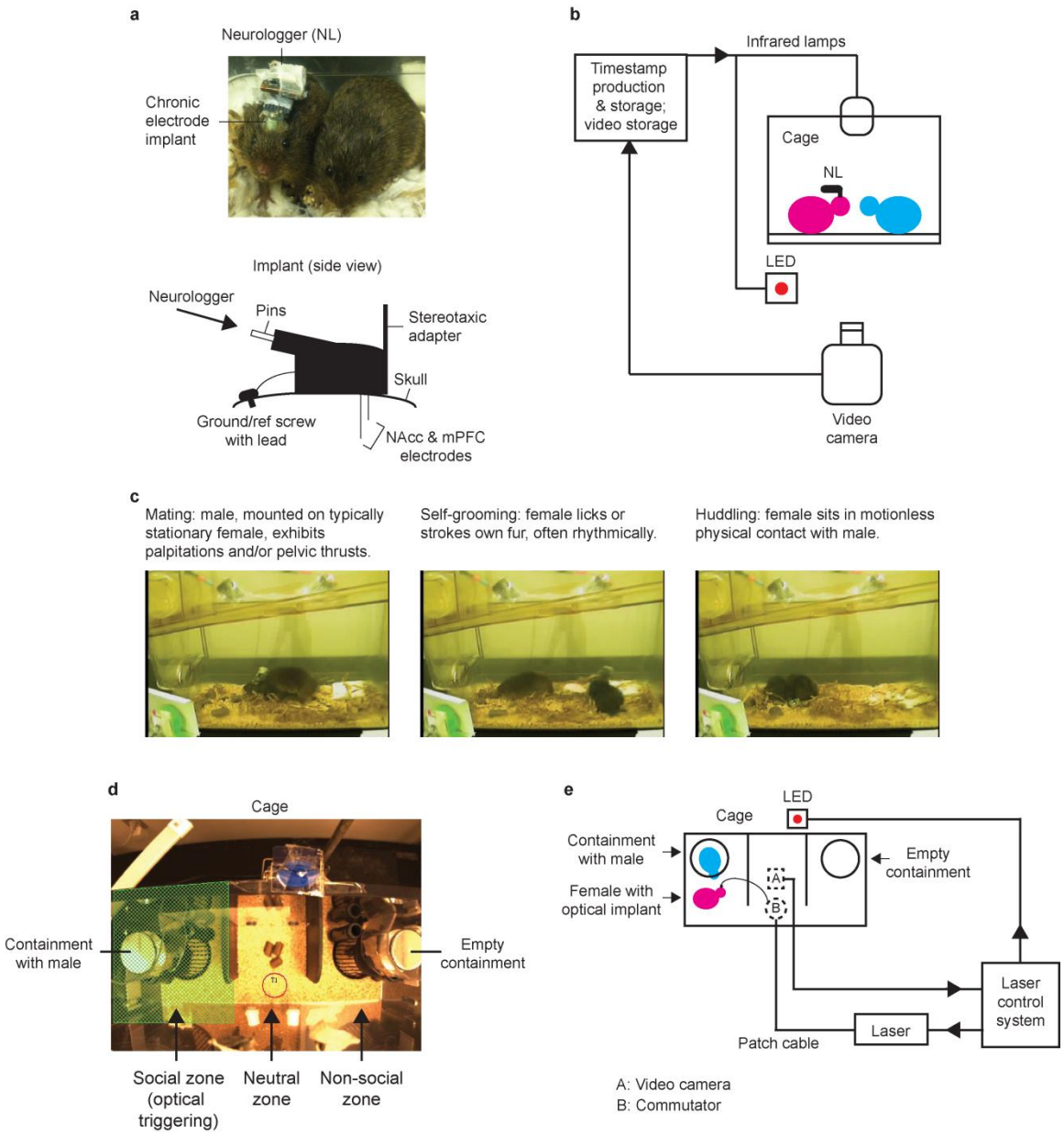

Figure 2.1 | Preparations for electrophysiological (a-c) and optogenetic (d-e) experiments. **a**, Neurologger recording device secured to a female during cohabitation with a male. The Neurologger interfaces with a chronic electrode implant targeting the mPFC and NAcc. **b**, Schematic of experimental setup. Simultaneous video and neural recording is synchronized by periodic timestamps. **c**, Summarized ethogram definitions of mating, self-grooming and huddling used to score experimental videos. **d**, Arena used for cohabitation in optogenetics experiments. The arena is divided into social, neutral, and non-social zones. Food is placed in the center of the neutral zone. The male is contained under a cup in the social zone, and the female, implanted with optical fibers, is allowed to freely explore the arena. Optical stimulation is triggered whenever she is in the social zone (green hatched area; red circle is visualization of tracking) for up to 1 hour within the cohabitation period. The social zone is defined as consistently as possible across experiments based on physical features of the arena. **e**, Schematic of cohabitation setup, additionally showing how the laser is controlled by video recording to automatically deliver optical stimulation when the female is in the social zone.

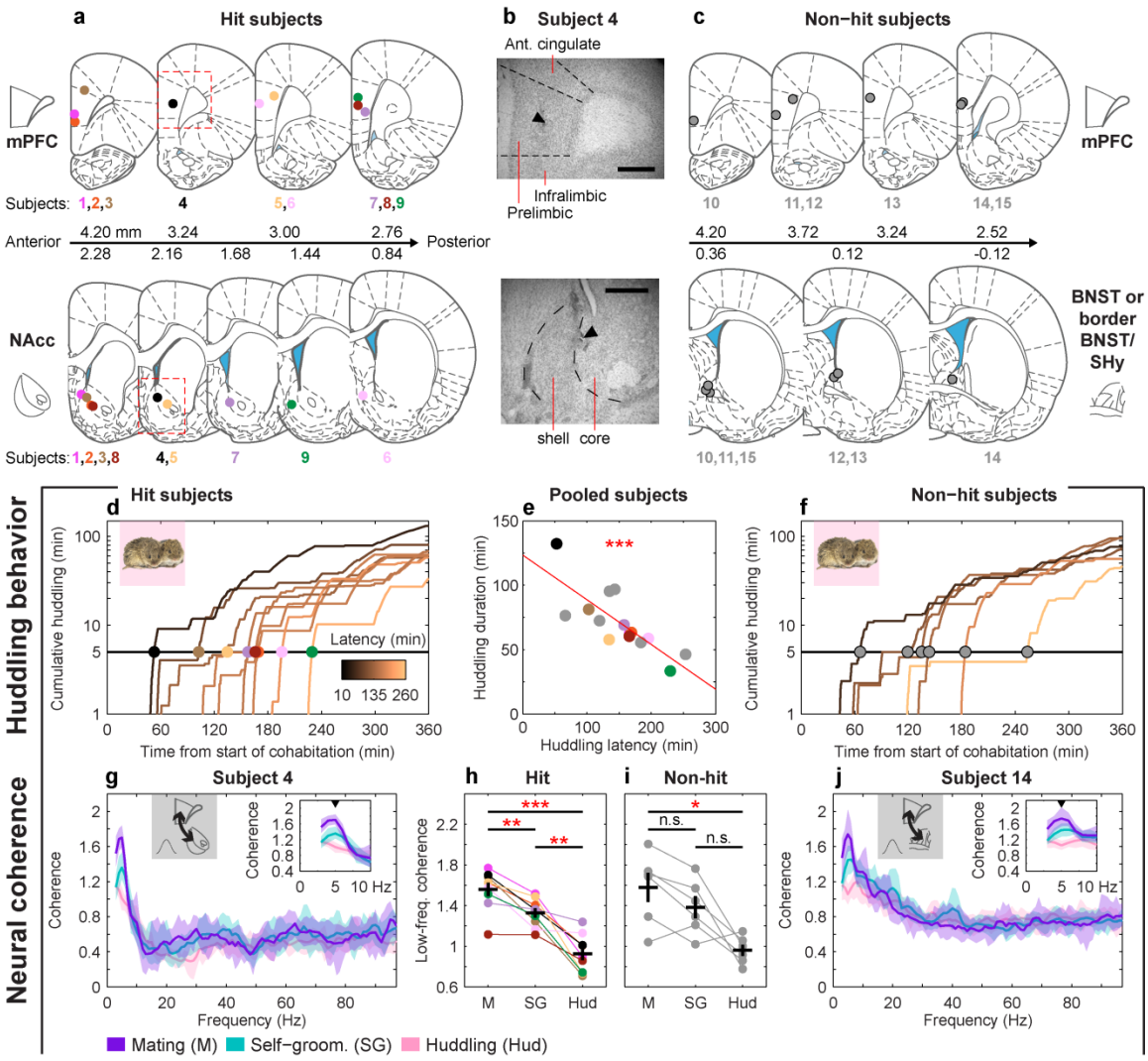

Figure 2.2 | Mating enhances low-frequency coherence across multiple brain areas. a, LFP recording sites in "hit" (n = 9) subjects targeting mPFC and NAcc, **b**, verified with electrolytic lesions (scale bar, 500 µm). Anterior/posterior locations of brain sections (units of rat brain atlas; see *Methods*) are indicated. **c**, Recording sites in "non-hit" (n = 6) subjects with electrodes in mPFC and within/bordering BNST. **d**, Cumulative huddling trajectories of hits and (**f**) non-hits during cohabitation; huddling latencies are indicated by dots color-coded by subject. **e**, Huddling latency is negatively correlated with total huddling duration over full cohabitation (n = 15; R^2 = 0.63, P < 0.001). **g**, Coherence spectra for example hit and (**j**) non-hit subjects, with insets showing low-frequency peaks during mating (5 Hz). **h**, 5 Hz coherence is significantly modulated by behavior in both hits ($F_{2,16}$ = 35.10, P < 0.001; post-hoc, M vs. SG, t_8 = 4.65, P = 0.005; M vs. Hud, t_8 = 6.73, P < 0.001; SG vs. Hud, t_8 = 5.10, P = 0.003) and (**i**) non-hits ($F_{2,10}$ = 12.43, P = 0.002; post-hoc, M vs. SG, t_5 = 2.44, P = 0.176; M vs. Hud, t_5 = 4.08, P = 0.029; SG vs. Hud, t_5 = 3.08, P = 0.082). Reported coherence P-values are Bonferroni-corrected for multiple comparisons (see *Methods*). Error bars show mean ± s.e.m. SHy: septohypothalamic nucleus.

.

posterior to the NAcc (within or bordering the bed nucleus of the stria terminalis (BNST); non-hit animals). Synchronized LFPs and video were acquired during a 6-hour cohabitation with a male. Mating, which accelerates bond formation (Williams et al., 1992), and side-by-side huddling, an index of bond expression (Ahern et al., 2009), were assessed as measures of affiliative behaviors during cohabitation. Self-grooming was assessed as a self-directed, high-motion control behavior.

Behaviors were variable from individual to individual, yet not different overall between hit and non-hit animal groups (Figure 2.3a). In particular, individuals varied in how quickly they began huddling (huddling "latency"), with those that started earlier going on to huddle more (Figure 2.2d-f). Accelerated huddling latencies were not simply explained by the quantity or timing of mating or self-grooming (Figure 2.3c), motivating me to ask whether mPFC-NAcc circuit activation could better explain variability in the timing of a switch towards more huddling.

Low-frequency drive from mPFC to NAcc can alter behavioral responses to environmental stimuli (Bagot et al., 2015; Britt et al., 2012), so I analyzed whether mPFC-NAcc connectivity increases during social behaviors that promote more affiliative responses to a partner. Low-frequency coherence, a common measure of functional connectivity, was significantly higher during mating compared to self-grooming and huddling (Figure 2.2g-h). Non-hit animals also showed significantly higher low-frequency coherence during mating compared to huddling (Figure 2.2i-j), indicating that mating generally enhances low-frequency connectivity across multiple brain areas, consistent with previous Fos studies in males (Johnson et al., 2016; Johnson et al., 2017).

To assess how this low-frequency connectivity modulates local activity within brain areas, I measured the interaction between low- and high (gamma)-frequency

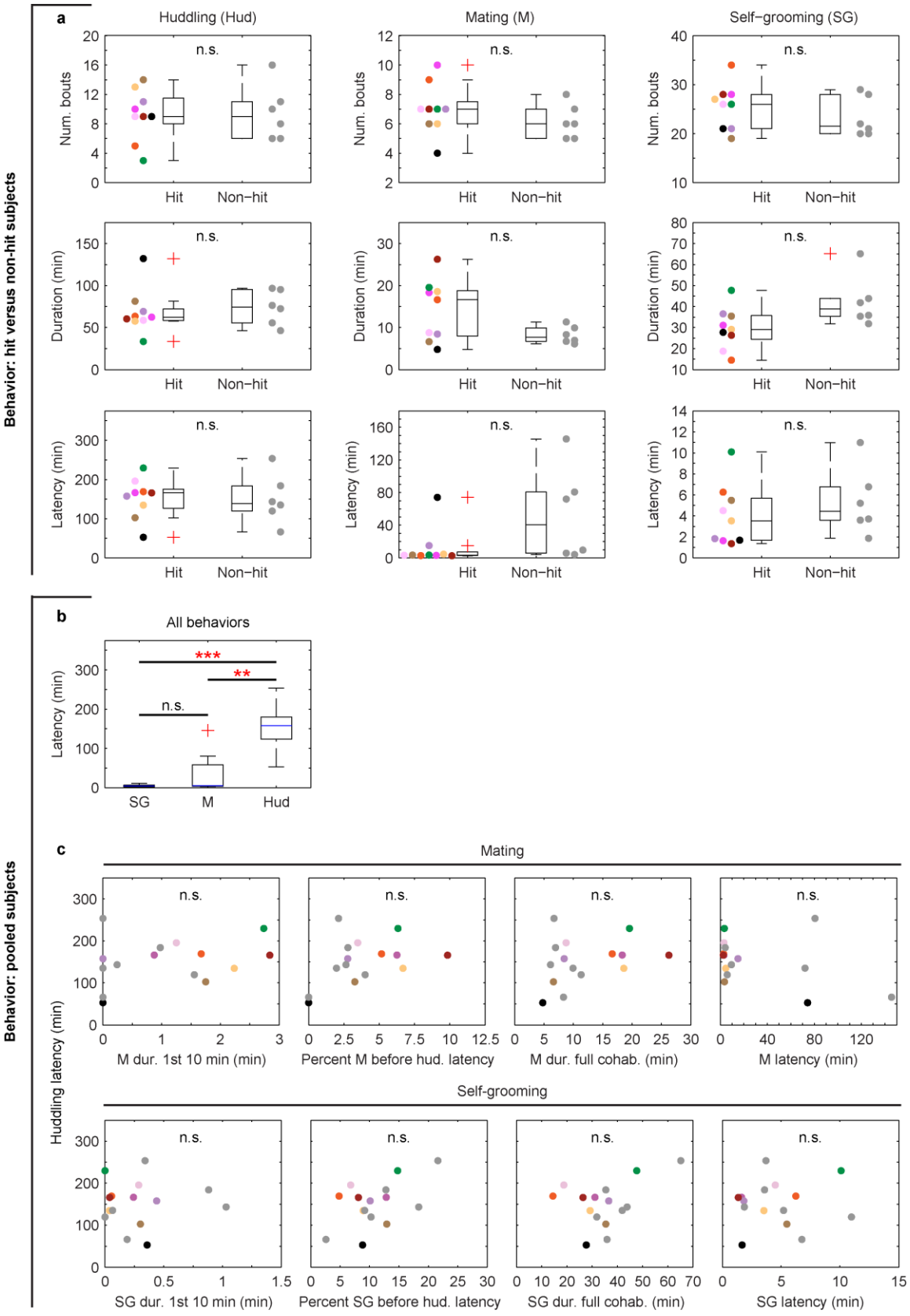
Behavior: hit versus non-hit subjects
a
Huddling (Hud)
Mating (M)
Self−grooming (SG)
Num. bouts
Duration (min)
Latency (min)
n.s.
Hit
Non−hit
Behavior: pooled subjects
b
All behaviors
***
**
n.s.
SG
M
Hud
c
Mating
Self-grooming
Huddling latency (min)
M dur. 1st 10 min (min)
Percent M before hud. latency
M dur. full cohab. (min)
M latency (min)
SG dur. 1st 10 min (min)
Percent SG before hud. latency
SG dur. full cohab. (min)
SG latency (min)

Figure 2.3 | Behavioral characterization of hit and non-hit subjects. a, Number of bouts, total duration, and latency for mating, self-grooming and huddling in hit (n = 9) and non-hit (n = 6) subjects. No significant differences exist between subject groups (all $P > 0.05$). **b**, Latency is modulated across behaviors (n = 15; $\chi^2(2) = 18.53$, $P < 0.001$, Friedman Test), with mating and self-grooming showing shorter latencies compared to huddling but similar latencies to each other (SG vs. Hud, $P < 0.001$; M vs. Hud, $P = 0.001$; M vs. SG, $P = 0.454$, Wilcoxon signed-rank). **c,** Measures of mating and self-grooming duration and latency do not correlate with huddling latency (n = 15; all $P > 0.05$). Reported P-values in **a-c** are Bonferroni-corrected for multiple comparisons (see *Methods*). Boxplots show median and interquartile range. Data points indicated by red cross refer to values whose distance from the top or bottom of the box is greater than 1.5 times the interquartile range.

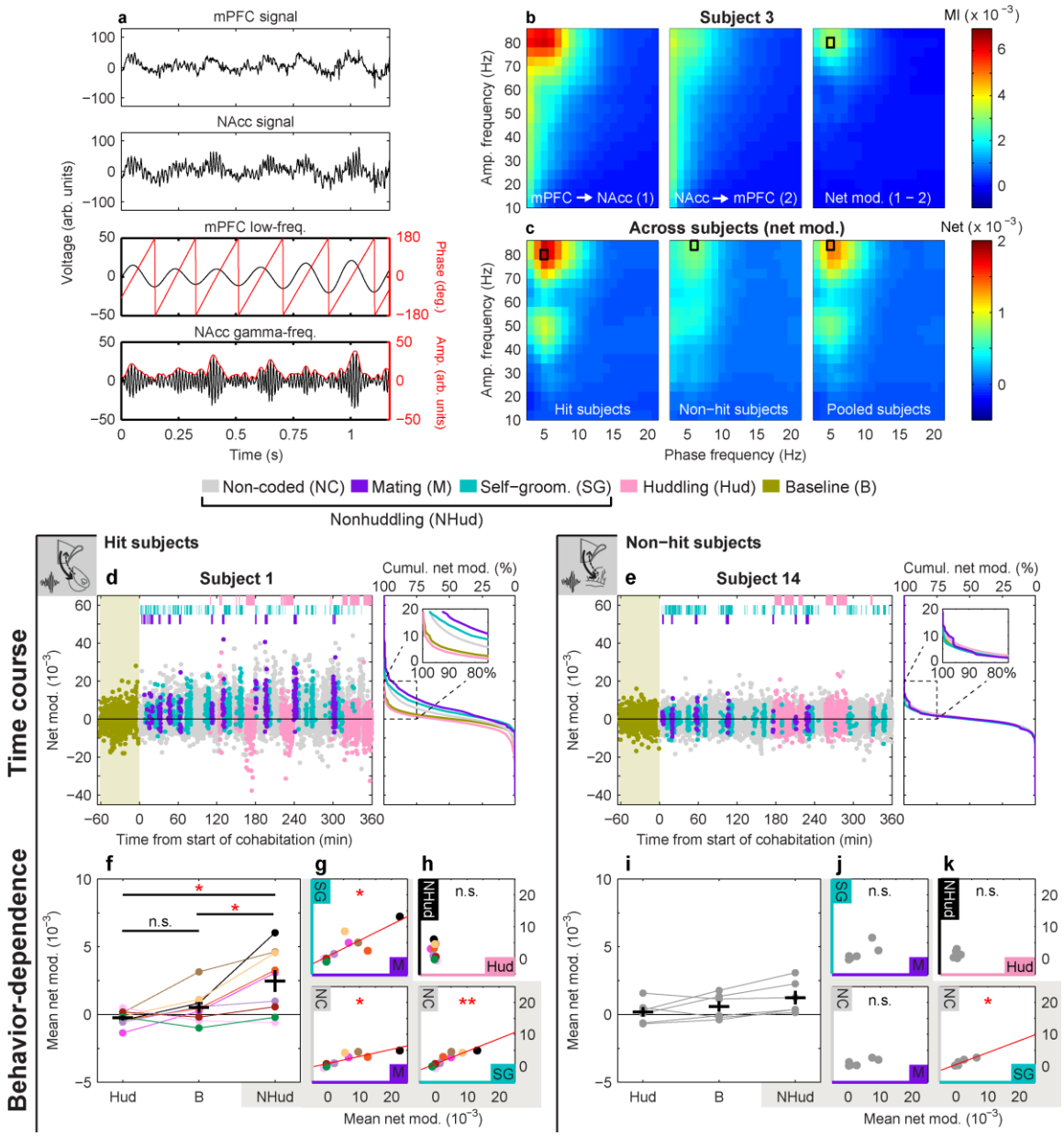

Figure 2.4 | mPFC-NAcc cross-frequency coupling is dynamically modulated and behavior-dependent. a, Example raw LFP signals of mPFC (top) and NAcc (upper middle), filtered into low-frequency (lower middle) and gamma-frequency (bottom) bands, shows gamma amplitude modulation by low-frequency phase. **b**, Modulation Index (MI) of phase-amplitude coupling for an example hit subject showing mPFC-to-NAcc (left) and NAcc-to-mPFC (middle) directions during cohabitation. "Net modulation" (right) is the difference in MI between directions. **c**, Mean net modulation for hit (left, *n* = 9), non-hit (middle, *n* = 6), or pooled (right, *n* = 15) subjects shows peaks when mPFC low-frequency phase modulates NAcc (or non-hit) gamma amplitude (indicated by black rectangle). **d**, Net modulation values (2-s, non-overlapping windows) sampled over a baseline solo period (gold region) and the 6-hr cohabitation for an example hit and (**e**) non-hit subject. Values that temporally overlap with mating, self-grooming and huddling behaviors (top hashes) are color-coded accordingly. All non-scored values are indicated as "non-coded," which together with mating and self-grooming represent "nonhuddling" values. Cumulative distributions of net modulation values coded by behavior are shown in right panel. **f**, Mean net modulation

across subjects during huddling, baseline and nonhuddling behaviors in all hits and (**i**) non-hits. Net modulation varies with behavior in hits ($F_{1.219,9.754}$ = 9.44, P = 0.010, Greenhouse-Geisser corrected; post-hoc, NHud vs. B, t_8 = 3.39, P = 0.028; NHud vs. Hud, t_8 = 3.17, P = 0.040; Hud vs. B, t_8 = 1.81, P = 0.322) but not non-hits ($F_{1.027,5.133}$ = 3.94, P = 0.102, Greenhouse-Geisser corrected). **g**, Pairwise correlations between net modulations for constitutive nonhuddling behaviors in hits (M vs. SG, R^2 =0.70, P = 0.015; M vs. NC, R^2 = 0.68, P = 0.018; SG vs. NC, R^2 = 0.78, P = 0.005) suggest individual variation in how strongly mPFC modulates NAcc. (**j**) Such individual variation was weaker in non-hits (M vs. SG, R^2 = 0.58, P = 0.240; M vs. NC, R^2 = 0.64, P = 0.172; SG vs. NC, R^2 = 0.83, P = 0.036). **h**, Nonhuddling and huddling net modulations were not correlated in either hits (R^2 = 0.10, P = 0.417) or (**k**) non-hits (R^2 = 0.06, P = 0.630). Reported P-values in **f**, **g**, **i** and **j** are Bonferroni-corrected for multiple comparisons (see *Methods*). Error bars show mean ± s.e.m.

oscillations across brain areas (Figure 2.4a). Gamma oscillations reflect local network activation (Buzsáki and Wang, 2012), including entrainment of FSIs within the ventral striatum (Berke, 2009; Kalenscher et al., 2010; van der Meer and Redish, 2009). In contrast, lower-frequency rhythms (e.g. delta, theta) can regulate gamma oscillations by phase modulating their amplitude (Lakatos et al., 2005), a phenomenon observed across brain areas (Tort et al., 2008). In both hit and non-hit groups, phase-amplitude coupling ("net modulation", Figure 2.4b-c) over the full cohabitation was maximal when low-frequency mPFC activity (5-6 Hz) modulated high gamma (80-84 Hz) activity in either the NAcc or non-hit area, motivating my focus below on this specific oscillatory channel for communication between regions.

Net modulation during the cohabitation and a pre-cohabitation solo baseline period were dynamically modulated, most prominently in hit animals (Figures 2.4d-e, 2.5). Positive values were consistent with Granger causality estimates showing elevated low-frequency drive from mPFC to NAcc (versus the reverse) during mating (Figure 2.6). Net modulation varied significantly with behaviors in hit animals only (Figure 2.4f,i). Net modulation during huddling was low and comparable to its level during baseline (Figure 2.4f), implying that huddling does not activate this reward-related circuit. Lack of activation was not likely from motionlessness, since animals were active and

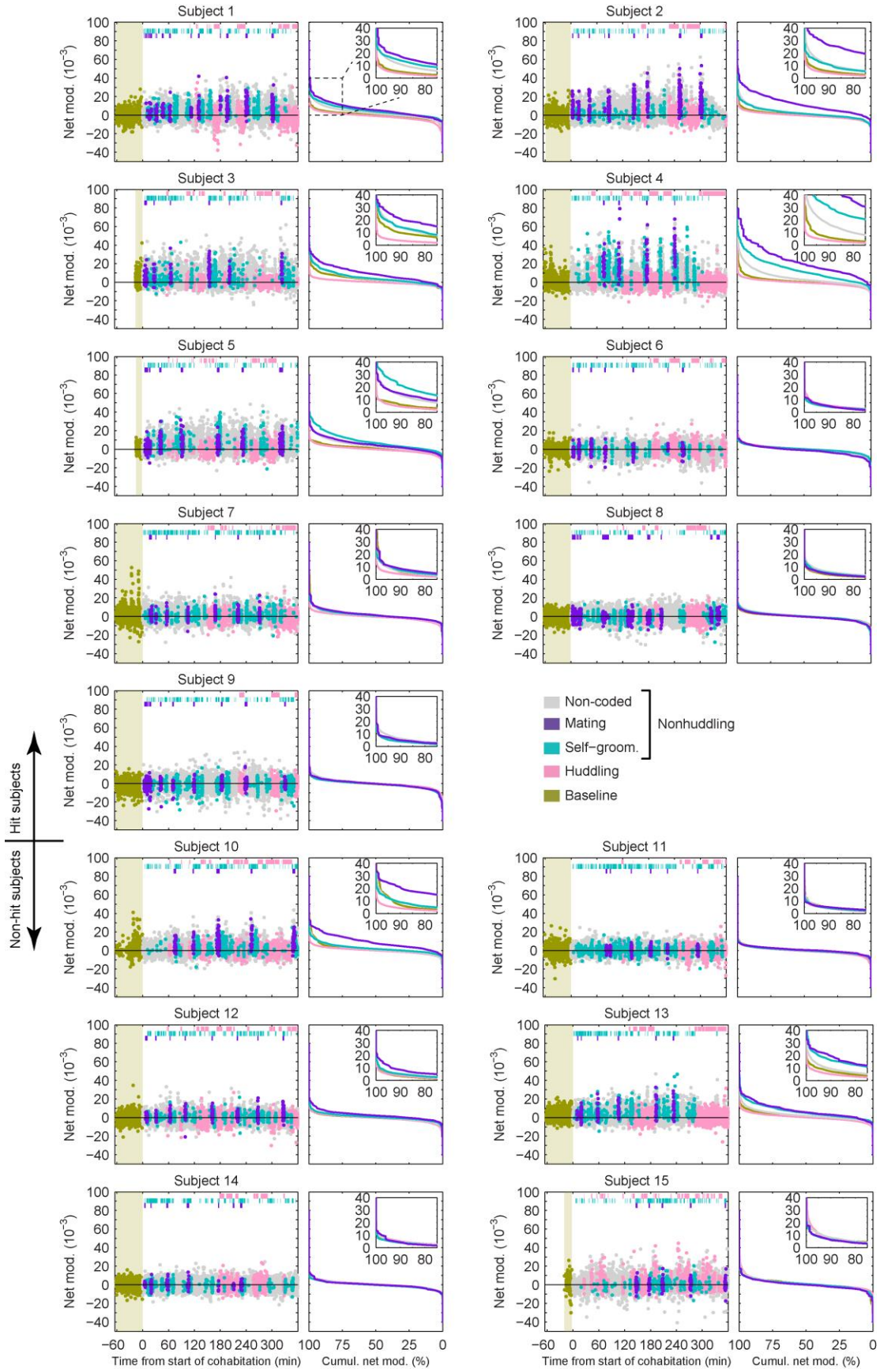
Subject 1
Subject 2
Subject 3
Subject 4
Subject 5
Subject 6
Subject 7
Subject 8
Subject 9
Subject 10
Subject 11
Subject 12
Subject 13
Subject 14
Subject 15
Net mod. (10^{-3})
Time from start of cohabitation (min)
Cumul. net mod. (%)
Non-coded
Mating
Self−groom.
Huddling
Baseline
Nonhuddling
Hit subjects
Non-hit subjects

Figure 2.5 | Net modulation data for all subjects. Net modulation values (2-s, non-overlapping windows) sampled over a baseline solo period (gold region) and the 6-hr cohabitation for all hit (#1-9) and non-hit (#10-15) subjects. Values that temporally overlap with mating, self-grooming and huddling behaviors (top hashes) are color-coded accordingly. All non-scored values are indicated as “non-coded,” which together with mating and self-grooming represent “nonhuddling” values. Cumulative distributions of net modulation values coded by behavior are shown in right panel for each subject.

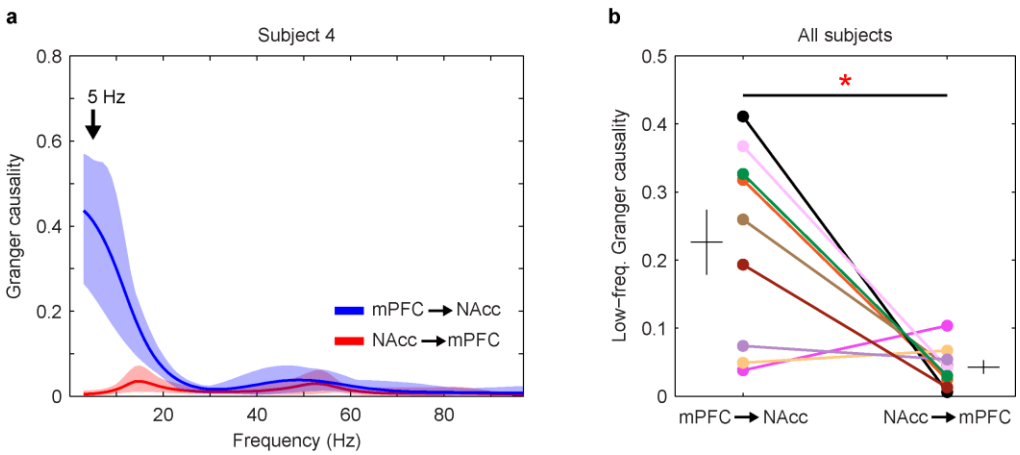

Figure 2.6 | Granger causality during mating. a, Granger causality spectra in the mPFC-to-NAcc and NAcc-to-mPFC directions for Subject 4. Solid lines show the mean and shaded areas show the mid-95 percentile range (2.5 to 97.5 percentiles) of the n = 40 estimates for a given brain-area direction (see *Methods*) **b**, Comparison of Granger causality at 5 Hz in the two directions across hit subjects (n = 9). Granger causality is significantly higher in the mPFC-to-NAcc direction (t_8 = 3.29, P = 0.011). Error bars show mean ± s.e.m.

investigative when alone. In contrast, net modulation outside of huddling (nonhuddling net modulation), consisting of mating, self-grooming and all non-coded behaviors, was significantly enhanced compared to both baseline and huddling. Mating, self-grooming, and non-coded net modulation, while not significantly different from each other (Figure 2.7), were instead correlated with each other (Figure 2.4g; no correlation between nonhuddling and huddling, Figure 2.4h). This indicates that nonhuddling net modulation reflects individual differences in mPFC-NAcc circuit activation, a result not trivially explained by variability in electrode placement (Figure 2.8a-b). Importantly, in the hit group only, individuals with greater nonhuddling net modulation over the full cohabitation, both overall and during individual nonhuddling behaviors, were significantly more likely to begin accumulating huddling faster (Figure 2.9a-b), while net modulation during huddling itself (consistently low across subjects, Figure 2.4f) did not correlate with the huddling latency (Figure 2.8e-f). Therefore, mPFC's specific modulation of NAcc activity explained how quickly individuals became affiliative.

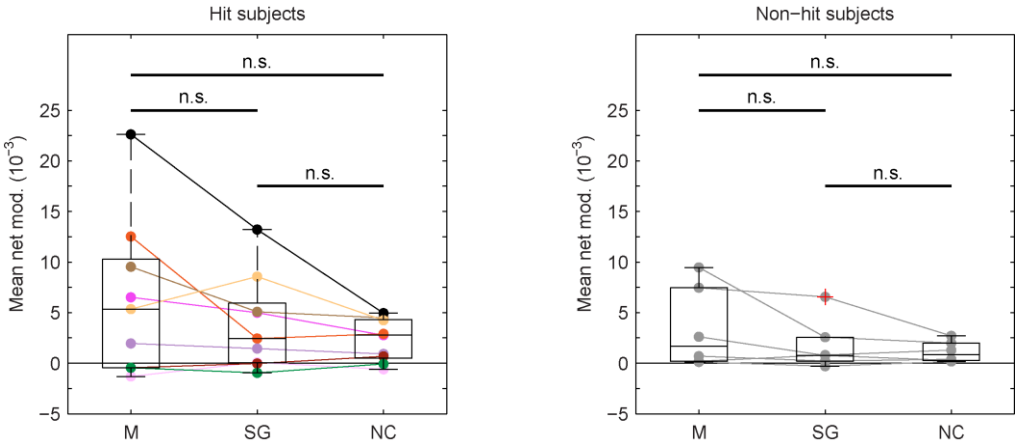

Figure 2.7 | Mean net modulation during mating, self-grooming and non-coded behaviors. **a**, The mean net modulation during mating, self-grooming and non-coded behaviors do not significantly differ from each other in either hits (n = 9) or (**b**) non-hits (n = 6) (all P > 0.05). Boxplots show median and interquartile range.

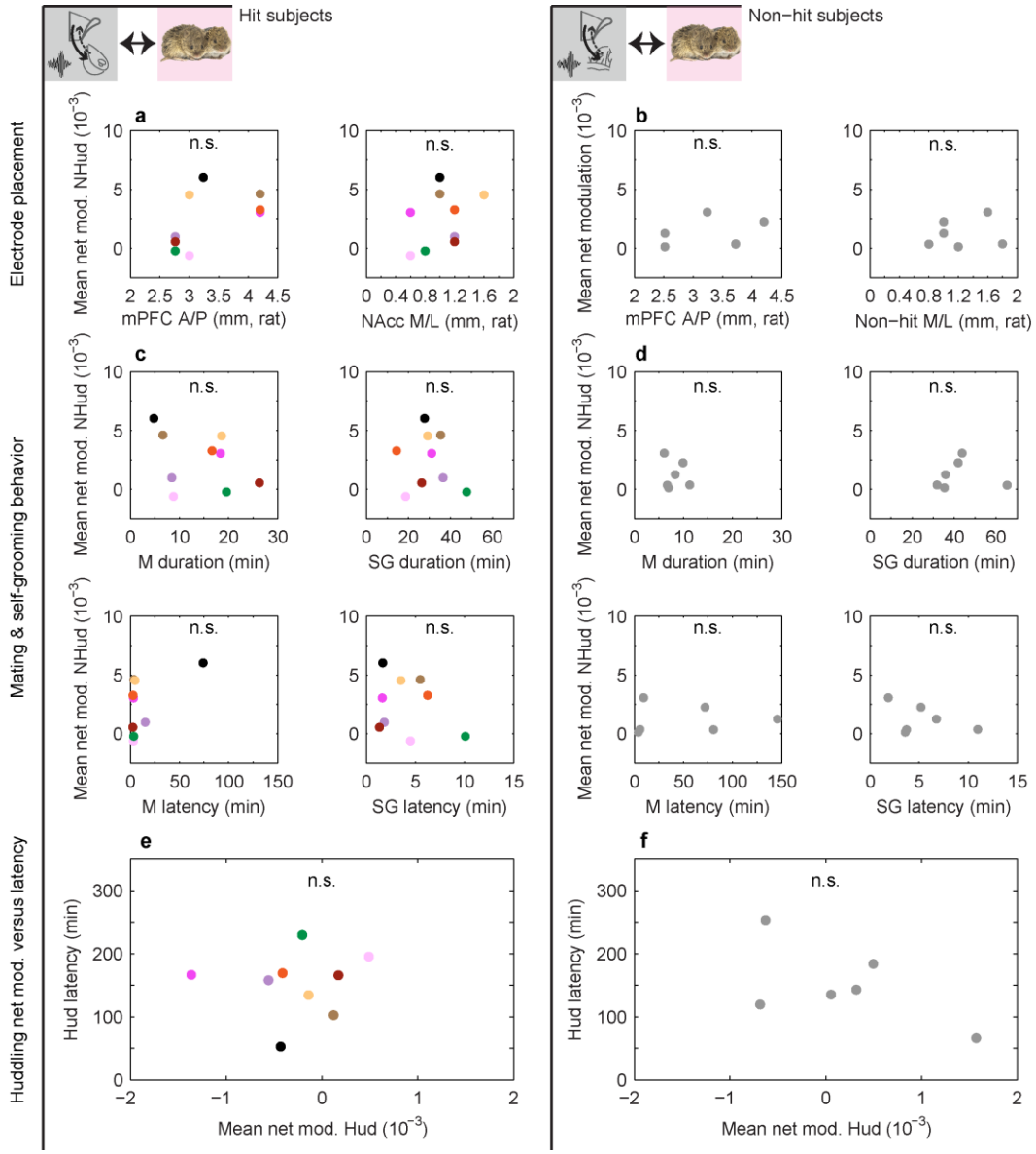

Figure 2.8 | Specificity of correlation between nonhuddling net modulation and huddling latency. a, Mean nonhuddling net modulation is uncorrelated with electrode placement (mPFC anterior-posterior (A/P) location or NAcc/non-hit medial-lateral (M/L); units of rat brain atlas) in both hits (n = 9) and (**b**) non-hits (n = 6) (all $P > 0.05$). **c**, Mean nonhuddling net modulation is uncorrelated with mating and self-grooming latency and total duration in hits and (**d**) non-hits (all $P > 0.05$). **e**, Mean huddling net modulation is uncorrelated with huddling latency in hits and (**f**) non-hits (all $P > 0.05$).

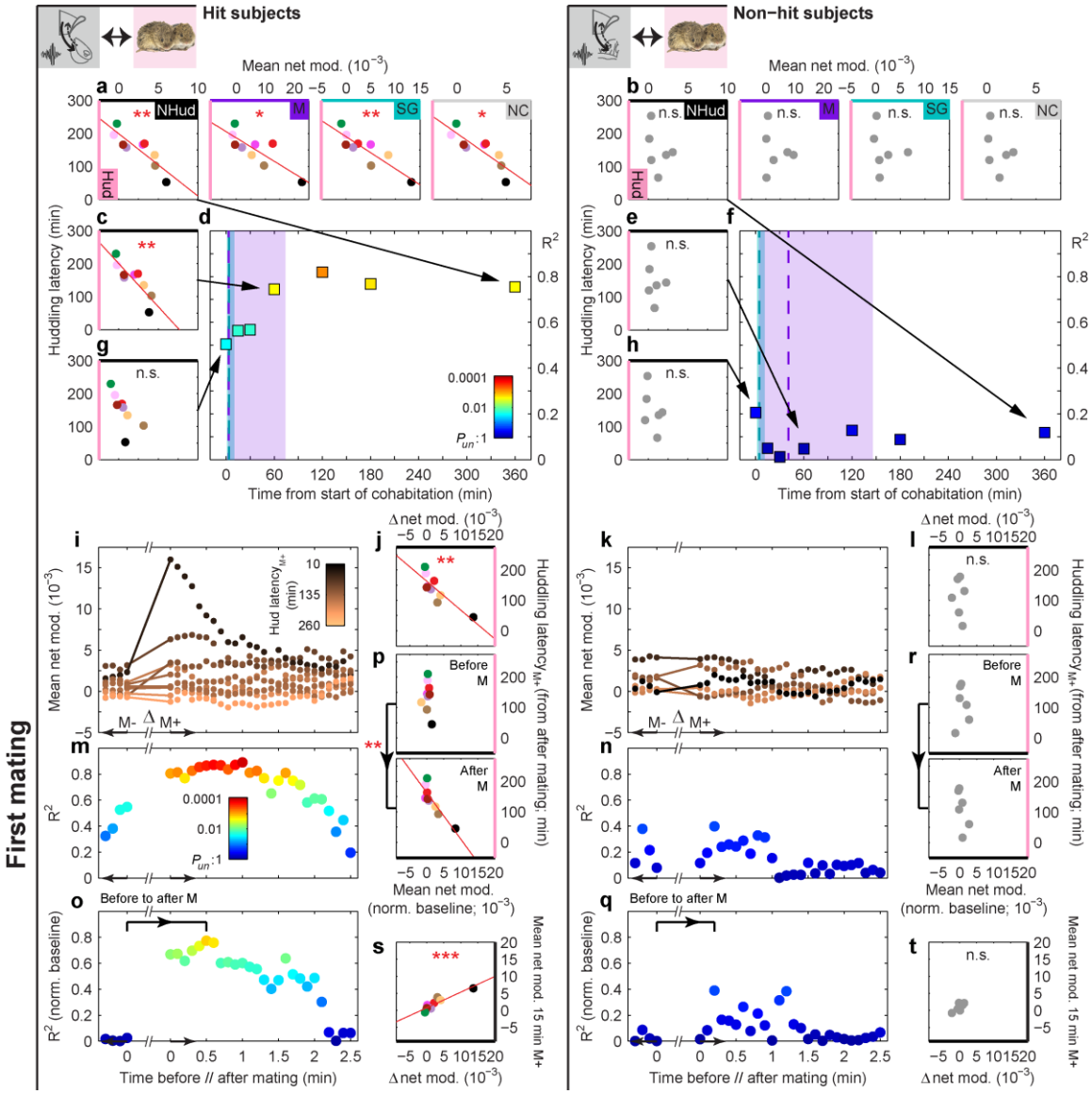

Figure 2.9 | mPFC-NAcc cross-frequency coupling correlates with huddling latency. **a**, Mean net modulation during nonhuddling behaviors, both individually (M, SG, NC; right) and pooled (NHud; left) during the full cohabitation correlate with the huddling latency in hits (M, R^2 = 0.67, P = 0.021; SG, R^2 = 0.77, P = 0.005; NC, R^2 = 0.72, P = 0.012; NHud, R^2 = 0.76, P = 0.007) but not (**b**) non-hits (M, R^2 = 0.03, P > 0.99; SG, R^2 = 0.04, P > 0.99; NC, R^2 = 0.14, P > 0.99; NHud, R^2 = 0.12, P > 0.99). **c**, Mean NHud net modulation during the first 60 minutes of cohabitation also correlates with the huddling latency in hits (R^2 = 0.74, P = 0.008) but not (**e**) non-hits (R^2 = 0.05, P > 0.99). **d**, Taking the mean NHud net modulation within increasing time windows from the start of cohabitation shows an increase in correlation strength (R^2) with huddling latency in hits but not (**f**) non-hits. Shaded regions and vertical dashed bars indicate the range and median of the latencies to first mating (purple) and self-grooming (green) across subjects. **g**, Mean baseline net modulation is not significantly correlated with the huddling latency in either hits (R^2 = 0.51, P = 0.096) or (**h**) non-hits (R^2 = 0.21, P > 0.99). **i**, Mean NHud net modulation values within 1 min moving windows (stepped by 0.1 min) before (M-) and after (M+) the first mating bout of hits and (**k**) non-hits. Each subject's values are color-coded by that subject's latency to huddle from the end of the mating bout (latency$_{M+}$). **j**, The change (Δ) in mean net modulation from immediately before to after the first mating bout (indicated by line segments

in **i**) negatively correlates with huddling latency$_{M+}$ in hits (R^2 = 0.72, P = 0.004) but not (**l**) non-hits (R^2 = 0.02, P = 0.766; line segments in **k**). **m**, The strength of the correlation between mean NHud net modulation and huddling latency$_{M+}$ increases from before to after mating and sustains a high level for ~2 min in hits but not (**n**) non-hits. **o-p**, This increase in hits is maintained, and significant (P = 0.002, permutation test on difference in R^2 (0.75) between bracketed time points), when subtracting out the mean baseline net modulation from the values before and after mating. **q**-**r**, Non-hits show no significant increase in correlation strength (P = 0.233, same permutation test as in **o-p**; observed R^2 difference of 0.39). **s**, The change in mean net modulation from immediately before to after the first mating bout correlates with the mean NHud net modulation in the 15 min after mating in hits (R^2 = 0.84, P < 0.001) but not (**t**) non-hits (R^2 = 0.58, P = 0.080). Plotted values in **d**, **f**, **m**-**o** and **q** are color-coded by the uncorrected P-value (P_{un}) of the correlation. Reported P-values in **a-h** are Bonferroni-corrected for multiple comparisons (see *Methods*).

To determine the temporal emergence of this correlation, I averaged the net modulation over increasing time windows from the start of cohabitation. Baseline net modulation was moderately, albeit non-significantly, correlated with huddling latency in hit animals, potentially indicating an individual's affiliative predisposition (Figure 2.9g). No predisposition was found in non-hit animals where the correlation was low and non-significant (Figure 2.9h). Nonhuddling net modulation became increasingly correlated with huddling latency by 60 minutes into the cohabitation in hit animals (Figure 2.9c-d), before most animals began huddling, but after experiencing their first mating bout (Figure 2.3b). No significant correlations emerged in non-hit animals (Figure 2.9e-f). Hence, even if a weak affiliative predisposition was reflected in the mPFC-NAcc circuit's baseline activation, early cohabitation experience further strengthened this specific circuit's correlation with huddling.

I next considered which early cohabitation behaviors could drive this strengthening. Mating typically occurred quickly (first bout range demarcated in Figures 2.3b, 2.9d,f), and its net modulation rose during cohabitation in hit animals, unlike self-grooming, another high net-modulation, early behavior (Figure 2.10). Given that mating promotes bond formation (Williams et al., 1992), I tested whether early mating improved

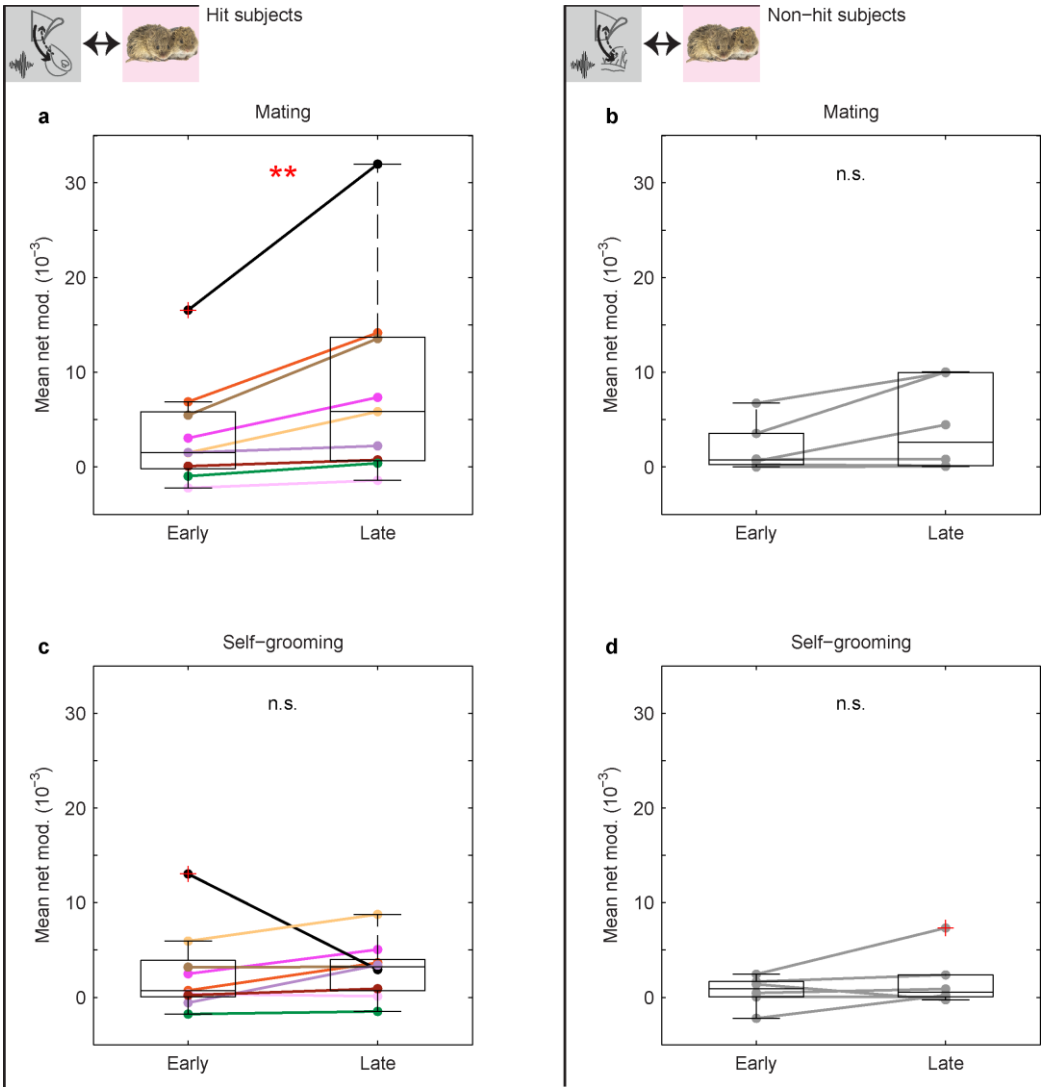

Figure 2.10 | Net modulation during early and late mating and self-grooming. a, Mean net modulation during mating increases over time in hits (n = 9, P = 0.008) but not (**b**) non-hits (n = 6, P = 0.438). **c**, Mean net modulation during self-grooming shows no significant change in either hits (P = 0.406) or (**d**) non-hits (P = 0.438). P-values in **a-d** are Bonferroni-corrected for multiple comparisons (see *Methods*). Mean early and late values for mating are derived from the first and last mating bouts. Mean values for self-grooming are derived from early and late self-grooming samples matched in number to the first and last mating bouts (see *Methods*). Boxplots show median and interquartile range.

the circuit's correlation with huddling. In hit animals only, the change in net modulation from immediately before to after the first mating bout predicted the latency to huddle from the end of the bout. Animals with larger increases in net modulation around the first mating, but not first self-grooming, more quickly began accumulating huddling (hits:

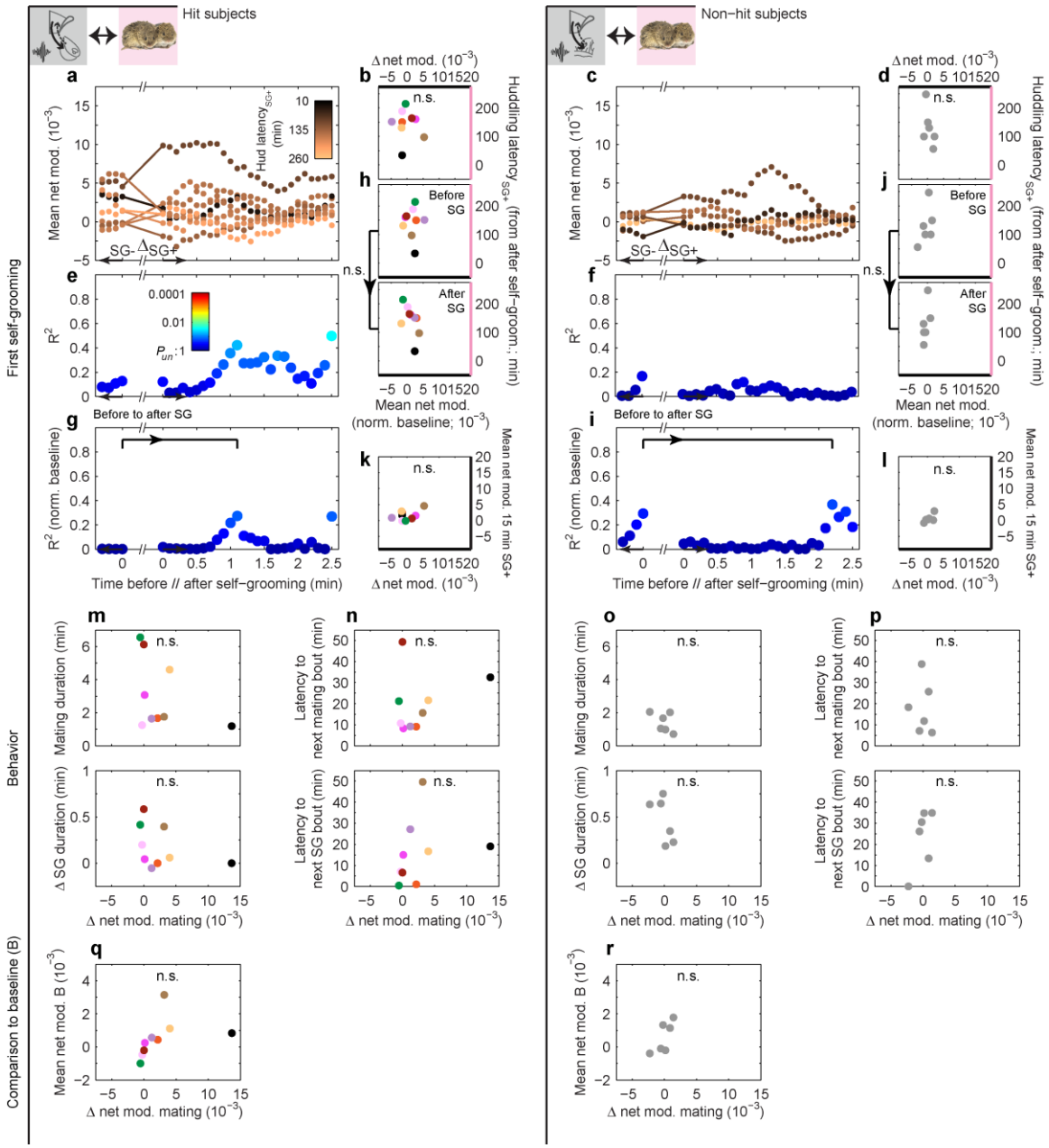

Figure 2.11 | Behavioral specificity of correlation between local change in net modulation around mating and huddling latency. a, Mean NHud net modulation values within 1 min moving windows (stepped by 0.1 min) before (SG-) and after (SG+) the first self-grooming bout of hits (n = 9) and (**c**) non-hits (n = 6). Each subject's values are color-coded by that subject's latency to huddle from the end of the self-grooming bout ($latency_{SG+}$). **b**, The change in mean net modulation from immediately before to after the first self-grooming bout (indicated by line segments in **a**) is uncorrelated with the huddling $latency_{SG+}$ in hits (R^2 = 0.01, P = 0.787) and (**d**) non-hits (R^2 = 0.27, P = 0.290; line segments in **c**). **e**, The strength of the correlation between the mean net modulation and huddling $latency_{SG+}$ shows no consistent increase in either hits or (**f**) non-hits. **g-h**, Subtracting out the mean baseline net modulation from the values before and after self-grooming confirms no significant increase in net modulation from before to after self-grooming in either hits (P = 0.164; permutation test on difference in R^2 (0.27) between bracketed time points) or (**i-j**) non-hits (P = 0.655; same permutation test as in **g-h**; observed R^2 difference of 0.07). **k**, The change in mean net modulation from immediately before to after the first self-

grooming bout is uncorrelated with the mean NHud net modulation in the 15 min after self-grooming in hits (R^2 = 0.24, P = 0.180) and (**l**) non-hits (R^2 = 0.55, P = 0.090). **m**, The change in net modulation around the first mating bout (Figure 2.9j,l) is uncorrelated with local behavioral parameters (change in self-grooming duration around bout and mating duration within bout) in hits and (**o**) non-hits (all $P > 0.05$). It is further uncorrelated with the latency to the next mating or self-grooming bouts (**n,p**) and the mean net modulation during the baseline solo period (**q,r**) in hits and non-hits (all $P > 0.05$). Plotted values in **e-g** and **i** are color-coded by the uncorrected P-value (P_{un}) of the correlation.

Figures 2.9i-j, 2.11a-b; non-hits: Figures 2.9k-l, 2.11c-d). Animals' change in net modulation was not simply explained by behaviors during and around mating (Figure 2.11m,o), and it specifically correlated with the latency to subsequent huddling (as opposed to subsequent mating or self-grooming, Figure 2.11n,p).

This mating-triggered change in net modulation augmented the circuit's correlation with huddling latency beyond predisposed levels. The magnitude of the change was not correlated with baseline levels (Figure 2.11q-r), suggesting a separate effect from any predisposition. Moreover, the correlation between local net modulation values (averaged over 1 minute) and huddling latency noticeably increased from the minute just before to up to ~2 minutes after mating (Figure 2.9m). Subtracting out individuals' baseline mean net modulation confirmed a significant augmentation (Figure 2.9o-p). No improvement was observed around self-grooming (Figure 2.11e,g-h), nor in non-hit animals around either mating or self-grooming (Figures 2.9n,q-r and 2.11f,i-j). In hit animals only, net modulation changes around mating, but not self-grooming, correlated with the subsequent net modulation, averaged up to the shortest huddling latency (i.e. 15 minutes after behavior) (Figures 2.9s-t, 2.11k-l). Hence, mating specifically altered both the temporally local and more sustained post-mating mPFC-to-NAcc circuit activation in a way that predicted subsequent huddling behavior: animals whose mPFC's modulation of NAcc was more strongly boosted went on to huddle faster,

thereby pointing to a new physiological source of individual variability in affiliative behavior.

To causally test the mPFC-NAcc circuit's sufficiency to accelerate huddling even without mating, I activated the circuit during a restricted cohabitation that prevented mating. This paradigm does not typically lead to pair bonding, as assessed in the laboratory by a later PPT (Ahern et al., 2009). In collaboration with Zachary Johnson in the Young Laboratory, I virally expressed Channelrhodopsin-2 (ChR2) or a control fluorophore (enhanced yellow fluorescent protein (EYFP)) in mPFC projection neurons. During the cohabitation, when the female entered a "social zone" containing a caged male, I optically stimulated (up to 1 hour) the mPFC-NAcc pathway at 5 or 6 Hz (Figures 2.1d-e, 2.12a-c, 2.13, 2.14), consistent with the frequency of peak mating coherence and net modulation. The ChR2 and EYFP groups showed comparable optical stimulation and time spent in each zone (Figure 2.12d), indicating that ChR2 activation did not induce coarse behavioral differences during the restricted cohabitation. However, in the PPT the following day, the ChR2 group showed significantly greater preference for the partner compared to the stranger (Figure 2.12e). Thus, low-frequency oscillatory drive from mPFC to NAcc can causally bias the emergence of affiliative behavior.

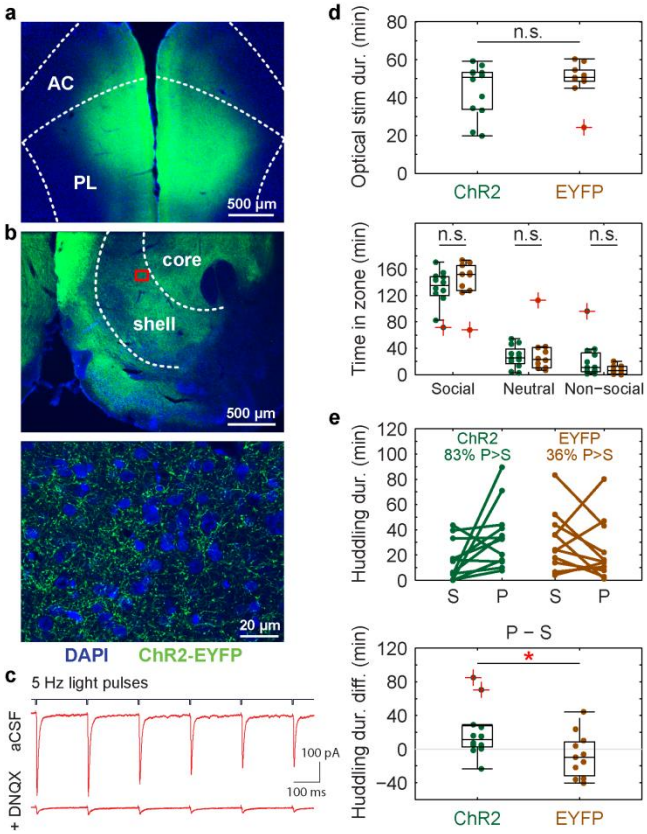

Figure 2.12 | Low-frequency optogenetic stimulation of mPFC-NAcc projections biases behavioral preference towards a partner. Example immunohistochemistry showing **a**, ChR2 expression in the mPFC (injection site, top image) and **b**, fibers projecting to the NAcc (stimulation site; middle and bottom images; bottom image is magnified view of area denoted by red box). ChR2 is tagged with enhanced yellow fluorescent protein (EYFP) for visualization. 4',6-Diamidino-2-Phenylindole, Dihydrochloride (DAPI) counterstain shows cell nuclei. **c**, Example whole-cell patch recording in a putative NAcc medium spiny neuron showing excitatory post-synaptic current evoked by 5 Hz light stimulation (average response to n = 5 pulse trains). Responses typically stabilized to 70-80% of initial amplitude. **d**, (Top) total optical stimulation and (bottom) time spent in each zone during cohabitation do not significantly differ between ChR2-expressing (n = 12) and control subjects (expressing EYFP only, n = 10; one subject missing due to data loss during cohabitation) (Stim, Cohen's d = 0.46, P = 0.298; Social, d = 0.41, P = 0.345; Neutral, d = 0.20, P = 0.698; Non-social, d = 0.68, P = 0.102). **e**, (Top) time spent with partner (P) versus stranger (S) during PPT for ChR2 (n = 12) and EYFP (n = 11) subjects. (Bottom) ChR2 subjects spent significantly greater relative time with the partner compared to stranger (d = 0.94, P = 0.034). Boxplots show median and interquartile range. Histology images in **a** and **b** prepared in collaboration with Zachary Johnson. Patch recording image in **c** prepared in collaboration with Steven Ryan (Rainnie Laboratory).

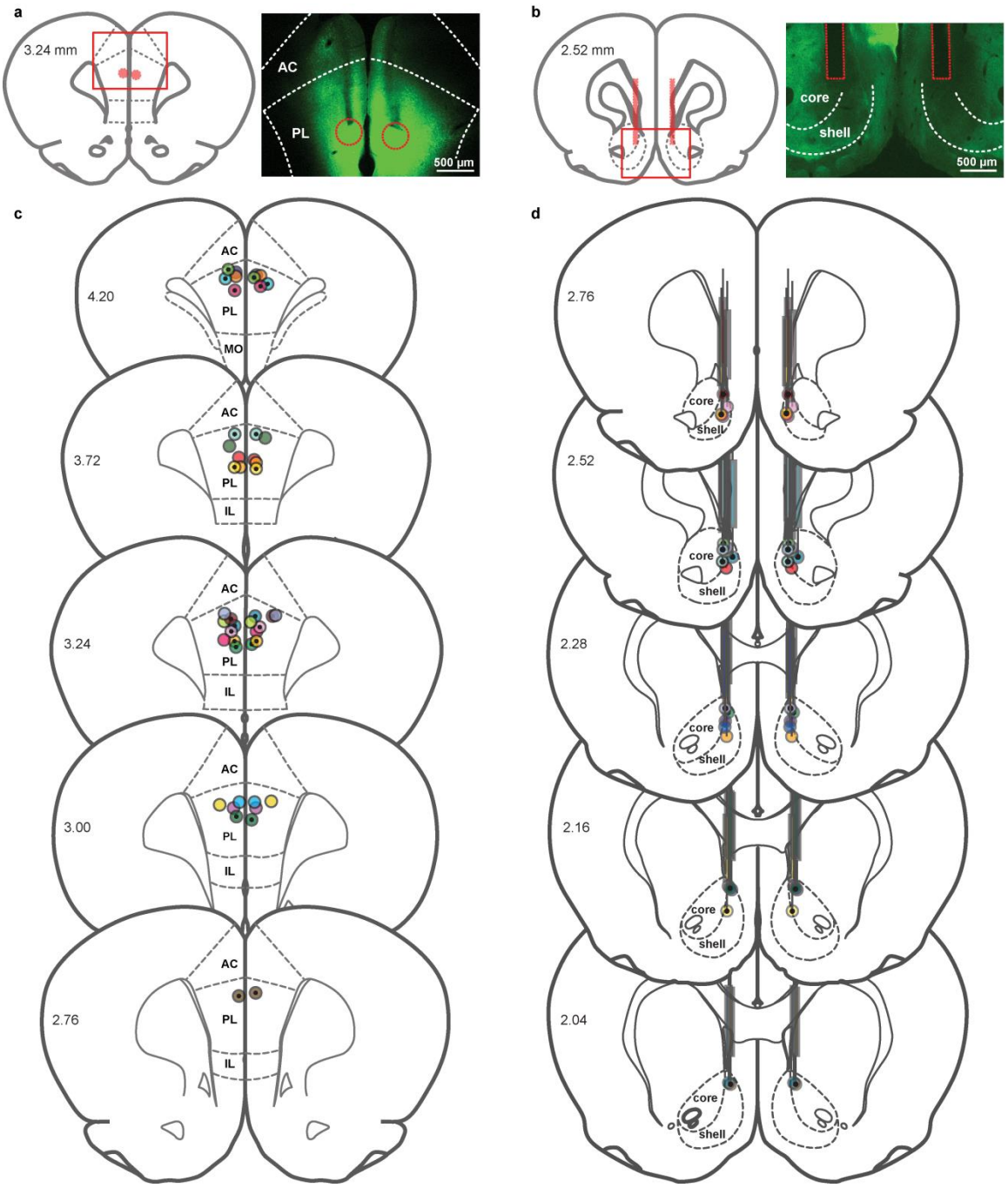

Figure 2.13 | Validation of virus injection and optical implant locations. a, Representative coronal sections showing estimated centers of bilateral virus injection and (**b**) optical implant placement for *in vivo* optogenetics subjects. Virus injection localization was based on minor tissue damage at the dorsal-most surface of the coronal section where the injection syringe initially entered the brain, the densest concentration of fluorescence and physical tracts of damage left by the injection syringe. Optical implant localization was based on physical tracts of damage left by the optical implant. Morphology of the corpus callosum was used to determine the anterior/posterior position of the injections and implants. **c**, Virus injection and (**d**) optical implant locations for all *in vivo* optogenetics subjects. ChR2-expressing subjects (n = 12) are indicated by circles with dotted centers. Control subjects (n = 11) are indicated by circles with empty centers. Each color is a separate subject, with two circles per subject (bilateral injection and optical

implant). All injection center locations fall within the PL and all optical implant locations fall within the medial NAcc. MO: medial orbital cortex. In **a-d**, the anterior/posterior location of each section (units of rat brain atlas) is indicated on left-hand side of section. This figure was prepared in collaboration with Zachary Johnson.

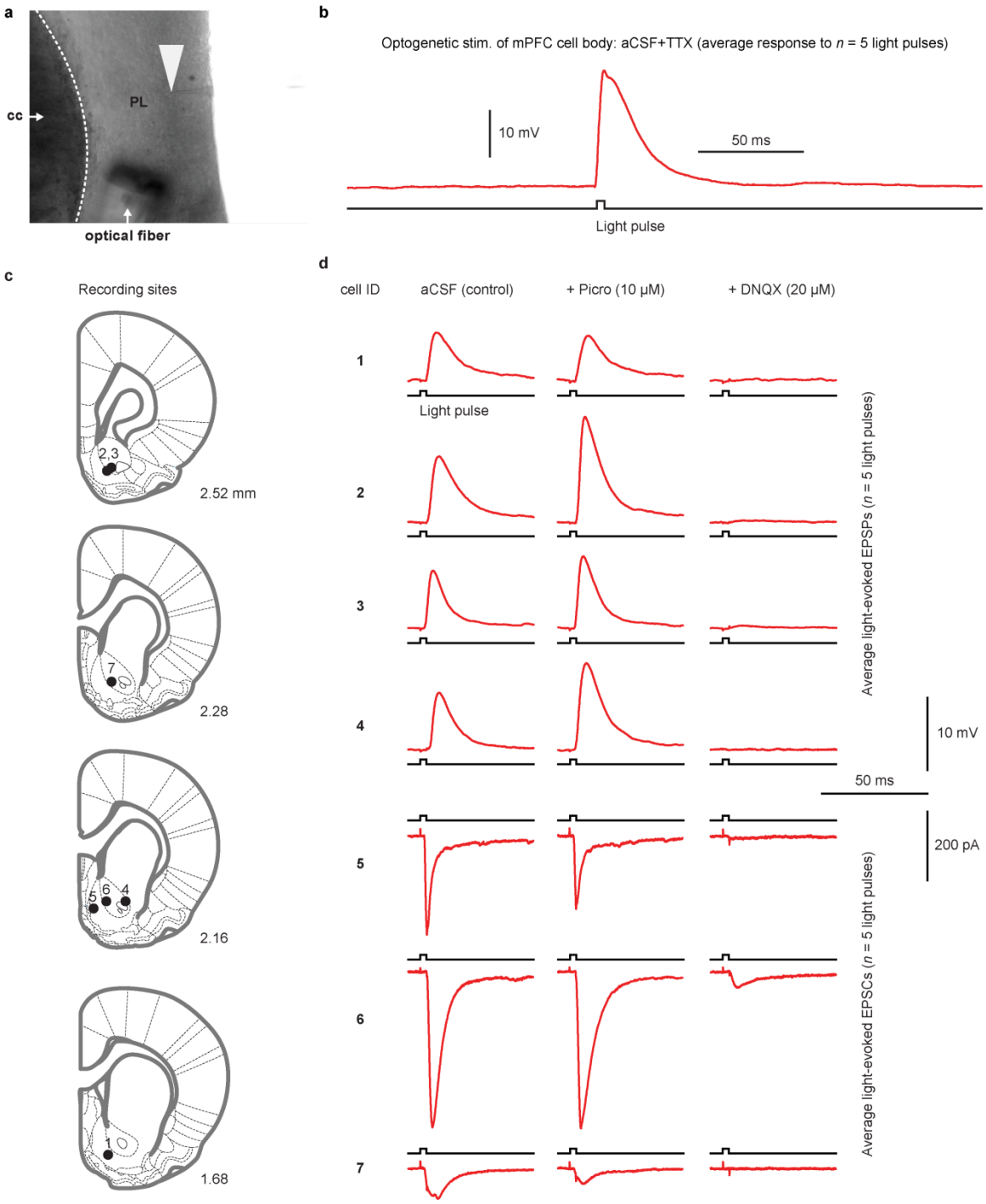

Figure 2.14 | Validation of light-induced electrophysiological responses in mPFC and NAcc. a, Representative image of whole-cell patch clamp recording from a prelimbic mPFC neuron cell body in slice preparation. Recording electrode (tip denoted with white arrowhead) is patched onto a cell, and an optical fiber is oriented towards the cell for optogenetic stimulation. cc: corpus callosum**. b**, Example light-evoked excitatory post-synaptic potential (average response to 5, 1ms light pulses; see *Methods*) in a prelimbic mPFC neuron in the presence of tetrodotoxin (TTX; 1 μM) to show a direct effect of light stimulation. **c**, Whole-cell patch clamp recordings were obtained from 7 putative medium spiny neurons (from *n* **=** 4 subjects) in the NAcc. Anterior/posterior location of each section (units of rat brain atlas) indicated on bottom-right

of section. **d**, Average electrophysiological responses (excitatory post-synaptic potentials (EPSPs; cells 1-4) or currents (EPSCs; cells 5-7)) to 5, 1 ms light pulses delivered onto the cell. Application of $GABA_a$ receptor blocker picrotoxin (Picro; second column) had no consistent effect on electrophysiological responses, whereas the AMPA-kainate receptor antagonist 6,7-dinitroquinoxaline-2,3-dione (DNQX; third column) disrupted them, indicating that electrophysiological responses were due to glutamatergic transmission. aCSF: artificial cerebrospinal fluid. This figure was prepared in collaboration with Steven Ryan.

2.3 Methods

2.3.1 Animals

All procedures were approved by the Emory University Institutional Animal Care and Use Committee. Experimental subjects (in *in vivo* electrophysiology, *in vivo* optogenetics, slice recording) were adult, sexually naive female prairie voles (*Microtus ochrogaster*) 76 to 154 days of age at the start of experiments. Animals were taken from our laboratory-bred colony derived from wild-caught Illinois stock. When possible, they were socially housed in same-sex duos or trios until implant surgeries (if performed), at which time they were separated and housed individually. Food (Lab Rabbit Diet HF #5326, LabDiet) and water were given *ad libitum* during a 14:10 hour light/dark cycle. Stimulus males used in behavioral experiments were adult, sexually experienced males under 1.5 years of age. Partners and strangers used in partner preference tests (PPTs; see below) were matched by age (within 61 days) and weight (within approximately 5 grams) for each female. Stimulus females used to prepare strangers were adult, sexually naive, socially housed females under 1 year of age.

Since this is the first study to my knowledge to apply *in vivo* electrophysiology and optogenetic approaches in behaving prairie voles, the target number of experimental subjects was chosen based on published studies in rodents using similar methods (Britt et al., 2012; Gruber et al., 2009a; Ross et al., 2009b).

2.3.2 Surgeries

All surgeries were done under isoflurane anesthesia. Anterior/posterior coordinates were referenced to Bregma, and dorsal/ventral coordinates were referenced to the top of the skull.

In *in vivo* electrophysiology experiments, females were ovariectomized to homogenize their hormonal state and chronically implanted with electrodes 10 to 20 days later. Electrodes were individual tungsten microelectrodes (1MΩ, FHC) stereotaxically targeted to the left medial prefrontal cortex (mPFC, anterior 2.3 to 2.4 (median: 2.35) mm, lateral 0.2 to 0.5 (median: 0.3) mm, ventral 2.5 to 2.7 (median: 2.6) mm) and either nucleus accumbens (NAcc, anterior 1.8 to 2.0 (median: 1.9) mm, lateral 0.8 to 0.9 (median: 0.8) mm, ventral 4.6 to 4.8 (median: 4.6) mm) or bed nucleus of the stria terminalis (BNST, anterior 1.05 to 1.9 (median: 1.1) mm, lateral 0.8 to 1.0 (median: 0.95) mm, ventral 4.45 to 4.6 (median: 4.5) mm), which receives direct mPFC projections in rodents (Gutman et al., 2012; Vertes, 2004). Electrodes were positioned in a fixed implant design (Figure 2.1a) that interfaced with a connector sitting on top of the skull. The connector in turn interfaced with the Neurologger recording device during experiments (see section 2.3.3 *Experiments*). A stainless steel ground screw (F000CE094, JI Morris) was placed in the right posterior cortex (anterior -2.6 mm, lateral -2.5 mm).

In *in vivo* optogenetics experiments, females underwent virus injection and optical fiber implant surgeries. Animals were bilaterally injected with an adeno-associated virus serotype 5 carrying either ChR2 tagged with yellow fluorescent protein under the control of calmodulin-dependent protein kinase II alpha promoter (AAV5-CaMKIIa-hChR2(H134R)-EYFP-WPRE-PA, 4-8.5x10^{12} viral molecules/mL, UNC Vector Core) or a control fluorophore lacking ChR2 (AAV5-CaMKIIa-EYFP, 4.4-5.2x10^{12} viral molecules/mL, UNC Vector Core) to the mPFC (anterior 2.4 mm, medial ± 0.3 mm, ventral 2.7 mm). Injection parameters were 500 nL per side, 5 min injection time and 5

min wait time between the end of injection and retraction of the injector to allow the virus to sufficiently diffuse from the injector needle. Animals were assigned to the ChR2 and control groups by randomly selecting the number of animals in a given cage that would receive ChR2 (either 1 or 2 in cages of 3; cages of 2 had 1 animal in each group by constraint) and counterbalancing across cages to produce as equal number of animals in each group as possible.

Approximately five weeks after virus injection, animals were implanted with a bilateral optical cannula (200 µm core diameter, 240 µm outer diameter, 0.22 NA, 4.5 mm fiber length, 1.5 mm pitch, flat tip, Doric Lenses) targeting the medial NAcc (anterior 1.9 mm, medial ± 0.75 mm, ventral 4.5 mm). The light transmission efficiency of the optical cannula was measured prior to implantation (S140C or S121C, PM100D, ThorLabs). Experiments started 6 weeks (42.0 ± 1.9 days (mean ± st. deviation)) following virus injection to allow for virus expression in mPFC afferents at the NAcc.

In slice electrophysiology experiments, females underwent the same virus injection surgery as described above, but received only ChR2 virus. Recording experiments in the mPFC and NAcc started 15 and 40-43 days following virus injection, respectively. A longer waiting time was used for NAcc recordings to allow for virus expression in mPFC afferents at the NAcc.

2.3.3 Experiments

Prior to behavioral experiments, all females (experimental subjects, stimulus females) were primed with estradiol benzoate (17-β-Estradiol-3-Benzoate, Fisher Scientific, daily injections of 1-2 µg dissolved in sesame oil starting 3 to 4 days prior to experiments) to induce sociosexual interest in males (Donaldson et al., 2010). The following experiments were performed once on independent experimental subjects).

2.3.3.1 Local Field Potential (LFP) Recording in Behaving Females During Cohabitation with a Male

LFPs were recorded from the mPFC and NAcc of behaving females using a battery-powered Neurologger (Etholm et al., 2010) chip (1-GB model, New Behavior AG). The Neurologger has 8 channels (4 neural data, 2 reference, 1 accelerometer, 1 infrared synchronization) and samples up to 500 Hz. We chose this over a higher-sampling rate, multichannel, tethered system due to the social nature and long recording duration of our paradigm, and the need to minimize the chance that the partner would interfere with recordings.

Prior to experiments, the Neurologger was programmed with sampling rate and data storage parameters and secured onto the connector on top of the animal's skull (Figure 2.1a). The device recorded and stored data during the experiment. It was disconnected at the end of the experiment to download data onto a computer for analysis. The sampling rate was 199.8 Hz for all subjects except Subject 3 (489.1 Hz). Both sampling rates covered an adequate frequency range for data analysis. Subjects were habituated to the device for at least one hour on the day before experiments.

On the morning of experiments, the female was briefly anesthetized under isoflurane to secure the Neurologger and then transferred to a clean cage in the testing room to habituate for at least 10-15 minutes (up to 1 hour). A stimulus male was also brought in to the testing room to habituate. This solo habituation period is referred to as the baseline period. At the end of the baseline, the male was added to the female's cage and the animals were cohabitated for 6 hours. Neural and video recording were performed throughout the baseline and cohabitation and synchronized using periodic timestamps delivered every 100 frames (3.3 seconds) from a Cleversys Topscan system running on a 32-bit Dell Precision T3500 computer. These timestamps were transmitted as infrared and visible light (LED) pulses that were registered in the Neurologger synchronization channel (samples) and the video recording (frames). The sample and frame indexes of these timestamps were detected and matched using custom-written

code in MATLAB (MathWorks). Experiments were performed under a Faraday cage to block 60-Hz electrical noise.

2.3.3.2 Optogenetic Stimulation in Behaving Females During Suboptimal Cohabitation with a Male

A combined video tracking and optical stimulation system was used to stimulate mPFC afferents in the NAcc of socially behaving female voles (Figure 2.1d-e). This consisted of a custom-designed, three-chambered Plexiglas arena divided into “social” (6” x 6”), “neutral” (center; 6” x 5.5”), and “non-social” (6” x 6”) zones. The social and non-social zones contained overturned perforated cups housing a male or remaining empty, respectively. A commutator (1x2 FC-FC, 0.22 NA, Doric Lenses) and video camera (Prosilica GC, Allied Vision Technologies) were positioned over the neutral zone. The commutator interfaced the laser (100 mW, 473 nm, fixed wavelength diode module, Cobolt) and a dual fiberoptic patch cable (200 µm core, 220 µm cladding, 900 µm jacket, Doric Lenses) that plugged into the optical cannula on the female, who had free access to the three zones. The female was tracked using an automated video tracking system (RV2 Video Processor, Tucker Davis Technologies) that detected a red marker positioned directly above her head on the patch cable. Optical stimulation was automatically triggered each time she entered the social zone (RV2 Video Processor and RZ5D Bioamp Processor, Tucker Davis Technologies, see Figure 2.1d-e) and occurred at a frequency of 5 or 6 Hz with pulse duration of 5 ms for as long as she remained in the social zone. Output from the optical cannula was approximately 30 mW (approximately 15 mW per implanted fiber) based on the output from the patch cable and the transmission efficiency of the optical cannula (measured prior to implantation). The tracking accuracy for time spent in the social zone (tracked time in social zone compared to human scoring) was at least 86.8% over subjects (tracking data for one

subject excluded due brief power outage causing data loss during cohabitation, see also *Statistics*).

On the day of experiments, the female was briefly anesthetized under isoflurane to connect the patch cable. She was then transferred to the three-chambered arena in the testing room, connected to the commutator, and allowed to habituate for 1 hour. At the same time, a non-implanted stimulus female was placed in a second, identical three-chambered arena in the same room and allowed to habituate. Two stimulus males were also brought into the room to habituate. At the end of the habituation, one stimulus male ("partner") was placed and contained in the social zone of the implanted female's cage, and the other male ("stranger") was placed and contained in the social zone of the non-implanted female's cage. This procedure was performed to ensure that the partner and stranger stimulus males received the same experience prior to partner preference testing.

Animals were cohabitated for 2.5 to 3 hours total. Within that period, stimulation was available for 1 hour starting from the first entrance of the implanted female into the social zone (laser disconnected at the end of this period). All subjects could therefore receive up to 1 hour of light stimulation, although the majority of animals spent some time outside of the social zone during this period and thus were not stimulated for the full hour (see Figure 2.12d, top). At the end of the cohabitation, the males and non-implanted stimulus female were removed and brought back to the colony. The implanted female was briefly anesthetized to disconnect the patch cable, placed in a clean cage, and returned to the colony. Because two cohabitation experiments were often run in a given day (typically starting in morning or early afternoon), the ordering of start times was counterbalanced within each experimental group to have similar number of animals starting in the morning and early afternoon.

The following day, the implanted female was tested in a 3-hour PPT with her partner from cohabitation and a stranger stimulus male. In this test, which was performed in a different room and cage from the cohabitation, the partner male was tethered with a plastic leash to one side of a three-chambered cage and the stranger male was tethered to the opposite side, as described previously (Ahern et al., 2009). The female, not connected to any optical cabling, was free to move around the cage and spend time with the partner and stranger. The amount of time the female spent in low-motion social contact (huddling) with the partner and stranger was measured with a Cleversys Topscan automated tracking system (movement criterion of < 0.04 (Ahern et al., 2009) for all subjects) and used to assess the female's preference for the partner (see section 2.3.6 *Statistics*). The side of the PPT cage on which the partner was tethered was counterbalanced within each experimental group to control for the partner's location in the testing room. Fresh bedding (Bed-o'Cobs Laboratory Animal Bedding ⅛", The Andersons) was used in each test.

2.3.3.3 Combined Electrophysiological Recording and Optical Stimulation in Slice Preparations of mPFC and NAcc Neurons of Females

Fifteen to 43 days following ChR2 virus injection, brain slices containing mPFC and/or NAcc were prepared as previously described (Ryan et al., 2012). Briefly, animals were decapitated under isoflurane anesthesia and brains rapidly removed and immersed in ice cold cutting solution perfused with 95% oxygen-5% carbon dioxide. Two-hundred μm-thick coronal sections containing mPFC and/or NAcc were then cut using a VTS-1000 vibrating blade microtome (Leica Microsystems). Slices were kept in oxygenated cutting solution at 32^0 C for 1 hour before being transferred to a recording chamber with regular aCSF. Slices were imaged using a Leica DM-LFS microscope (Leica Microsystems) captured with SimplePCI software (Hamamatsu Corp.) for areas of strong

fluorescence within the target region of interest (mPFC or NAcc), and recordings performed as follows:

2.3.3.3.1 NAcc

Putative medium spiny neurons were visually identified, patched with a thin-walled borosilicate glass-patch electrode, and held at -70 mV with either DC current injection in current clamp (*n* = 4 cells) or voltage clamp (*n* = 3 cells) configuration. Recording techniques and equipment were as previously described (Ryan et al., 2012). Excitatory post-synaptic potentials (or currents) were then evoked with optical stimulation via an optical fiber connected to a solid-state laser (Shanghai Laser & Optics Century Co.) and oriented towards the cell (200 μm core, 488 nm, 0.9-3.4 mW measured at end of fiber). Stimulus trains were either 5 Hz (6 pulses at 5 Hz, 1 ms pulse duration, repeated every 4 seconds for a total of 5 pulse trains) or individual light pulses (1 ms pulse duration, repeated every 4 seconds for a total of 5 pulses) used to compute an average electrophysiological response.

Drugs were applied by gravity perfusion at the required concentration in the circulating aCSF. Drugs used were picrotoxin (Picro; 10 μM) and 6,7-dinitroquinoxaline-2,3-dione (DNQX; 20 μM). All drugs were acquired from Tocris and stored frozen as concentrated stock solutions in distilled water (dH_2O) except DNQX, which was made in 50% dimethyl sulfoxide. In recordings in the NAcc, Picro and DNQX were added serially, in that order, with recordings between applications. Following experiments, mPFC slices from the same subjects were stored for histological verification of virus expression (see section 2.3.4 *Histology*).

2.3.3.3.2 mPFC

Recordings in prelimbic mPFC were performed as described above, with the exception that the recorded cells were putative pyramidal neurons and maintained at a membrane potential of -60 mV. Cells were recorded from in the presence of tetrodotoxin

(TTX; 1 µM). TTX was acquired from Tocris and stored frozen as a concentrated stock solution in dH_2O.

2.3.4 Histology

2.3.4.1 *In Vivo* Electrophysiology

At the end of experiments, electrode-implanted females were deeply anesthetized under isoflurane and electrolytic lesions performed at each electrode site (10 µA for 40-45 seconds, Midgard Precision Current Source, Stoelting Co.). The animals were then euthanized with carbon dioxide. The brain was removed, stored 1 to 2 days in 1x phosphate buffered saline (PBS) containing 4% paraformaldehyde (PFA) at 4^0 C, and transferred to 1x PBS containing 30% sucrose at 4^0 C until fully fixed. Forty µm-thick sections were prepared on a freezing sliding microtome (Microm). Sections were stored in cryoprotectant, mounted on slides and Cresyl Violet-stained. Slides were coverslipped and then imaged on an Eclipse E800 light microscope (Nikon Instruments). Lesion sites were identified and the section was matched to the most anatomically similar plate in the Paxinos and Watson Rat Brain Atlas (Paxinos and Watson, 2009). Anatomical landmarks used to match the sections to the atlas included the morphology and position of the corpus callosum and anterior commissure. Subjects with NAcc electrodes within or on the medial border of the NAcc were included as hit subjects (*n* = 9; see Figure 2.2a). Subjects with electrodes posterior to the NAcc (within or bordering BNST) were included as non-hit subjects (*n* = 6; see Figure 2.2c).

2.3.4.2 *In Vivo* Optogenetics

Tissue processing: At the end of experiments, subjects were deeply anesthetized under isoflurane and transcardially perfused with 40 mL 1x PBS followed by 40 mL 4% PFA in 1x PBS at a rate of approximately 4 mL per minute. Following perfusion, brains were rapidly extracted and post-fixed overnight in 4% PFA in 1x PBS and were then transferred to 1x PBS containing 30% sucrose and 0.5% sodium azide. Forty µm-thick

coronal sections were collected using a freezing sliding microtome (Microm) and were stored in 1x PBS containing 0.5% sodium azide until immunohistochemical staining.

Immunohistochemistry: All sections from both treatments were subjected to fluorescent immunohistochemical labeling for EYFP. Sections were washed in 1x PBS and blocked with 1x PBS containing 2% normal goat serum (NGS, Fitzgerald) for 1 hour before primary incubation with anti-GFP primary antibody (1:1,000, chicken polyclonal, Abcam ab13970) in 1x PBS containing 0.2% Triton-X (1x PBST) and 2% NGS for 48 hours at 4° C. Following primary incubation, sections were washed in 1x PBST and incubated in secondary antibody conjugated to a green fluorophore (1:1,000, goat polyclonal anti-chicken, Alexa Fluor 488, ab150169) for 4.5 hours in 1x PBST containing 2% NGS. Sections then underwent final washes in 1x PBS before being mounted onto slides. Slides were allowed to dry overnight and were then coverslipped with Vectashield Antifade Mounting Medium with DAPI (H-1200, Vector Labs).

Fluorescent Microscopy: Confocal images were collected using an Orca R2 cooled CCD camera (Hamamatsu Photonics) mounted on a Leica DM 5500B microscope (Leica Microsystems) equipped with a CSU10B Spinning Disk (Yokagawa Electronic Corp.) and captured with Simple PCI imaging software (Hamamatsu Photonics). Additional fluorescent images were captured using a QI Imaging Fast 1394 12-bit camera mounted on an Eclipse E800 fluorescent microscope (Nikon Instruments) and captured using MCID Imaging software.

2.3.4.3 Slice Electrophysiology

Tissue processing: Following electrophysiological recordings in NAcc, 200 µm-thick coronal sections containing the recorded slice as well as sections from the same subject containing mPFC were stored 1 to 2 days in 1x PBS containing 4% PFA at 4^0 C, and transferred to 1x PBS containing 30% sucrose at 4^0 C until fully fixed. Immediately prior to mounting, sections were transferred into and washed in 0.1x PBS and were

directly mounted onto slides. Mounted sections were allowed to dry overnight and were then coverslipped using Vectashield HardSet Antifade Mounting Medium with DAPI (Vector Labs; H-1500). Dense expression of the ChR2-EYFP transgene in both the mPFC and the NAcc was used as a criterion for inclusion and was confirmed at 60x magnification using an Eclipse E800 fluorescent microscope (Nikon Instruments) for all subjects. acquired from Tocris and stored frozen as a concentrated stock solution in dH_2O.

2.3.5 Data Analysis

Following electrophysiology experiments, subject records (*n* = 15 total; 9 hit subjects, 6 non-hit subjects) were added to a custom relational database (Microsoft Excel) used to index animals during analysis. Cohabitation videos were then behaviorally scored and the corresponding neural data extracted and analyzed. Subjects were labeled as hits (1 through 9) or non-hits (10 through 15). They were ordered by the relative anterior/posterior position of their mPFC recording electrode, with "1" being the most anterior of the hit group, and "10" being the most anterior of the non-hit group.

2.3.5.1 Behavioral Scoring

An ethogram was developed to define mating, self-grooming and huddling behaviors occurring in these experiments (see Figure 2.1c). These were then scored in experimental videos (Observer XT10) and matched to neural data using linear regression to the most adjacent timestamps (see synchronization procedure described above). For consistency and reliability in scoring, two individuals trained on a test video and scored the experimental videos blindly to each other. The percent agreement between the two scoring records of a given behavior, calculated as the percentage of total frames scored consistently for that behavior (i.e. occurring or not), was at least 97.9% for mating, 94.6% for self-grooming and 92.3% for huddling over all hit subjects and 99.5% for mating, 95.8% for self-grooming and 91.1% for huddling over all non-hit

subjects. Therefore, we used the intersection of each behavior's scoring within the two records as the measure of that behavior. Contiguous segments of intersected scoring are referred to as "epochs" and are used in the following analyses of behavioral scoring.

2.3.5.1.1 Trials

Trials were extracted from behavior epochs that were at least 5 seconds long and for which the individual scoring records started within 1 second of each other (with the exception of huddling, which used a criterion of starting within 5 seconds due to a slower onset of the behavior). Trials were defined as the first 5 seconds of the behavior epochs. Trials were further restricted to be within the 6-hr cohabitation. The number of 5-second trials of mating for all subjects were (ordered by ID) 46, 72, 22, 15, 55, 26, 12, 89, 21, 47, 23, 48, 21, 21 and 24. The number of 5-second trials of self-grooming were 47, 37, 59, 19, 21, 37, 57 ,17, 34, 49, 73, 58, 42, 42 and 11. The number of 5-second trials of huddling were 45, 24, 24, 37, 26, 48, 41, 13, 4, 51, 27, 57, 44, 14 and 25.

2.3.5.1.2 Rasters

For cross-frequency coupling analyses, the cohabitation was broken into 2-s non-overlapping time segments. Time segments fully overlapping within an epoch of mating, self-grooming or huddling were labeled as that behavior. All remaining time segments were labeled as "non-coded". Time samples labeled as mating, self-grooming and non-coded together made up "nonhuddling" time samples.

2.3.5.1.3 Bouts

To capture sequences of a given behavior, the distances between adjacent behavior epochs were computed and pooled to create a distribution of distances. A single- or two-term natural exponential function was fit to this distribution. Writing the exponential function in the form of Equation 1,

$$f(x) = a * \exp(-bx) + c * \exp(-dx) \quad (1)$$

the fitted values of *a* for mating, self-grooming and huddling were 23320, 15222 and 5347 minutes, respectively. The values of *b* (first-term decay constant) were 5.315, 3.089 and 3.481 minutes, respectively. The values of *c* were 0, 472.6 and 21.17 minutes, respectively. The values of *d* (second-term decay constant) were 0, 0.433 and 0.133 minutes, respectively. For each behavior, the decay constant of the largest contributor to the fitted function (5.315, 3.089, 3.481 minutes for mating, self-grooming and huddling, respectively) was used as the threshold distance between epochs for inclusion within a given bout.

2.3.5.1.4 Latency

Latency was calculated for each behavior as the delay from a given reference point within the experiment (e.g. start of cohabitation) to a later reference point within a behavior (e.g. bout start).

2.3.5.1.5 Duration

For each behavior, epochs within a given time window (e.g. full cohabitation, smaller time windows) were pooled to compute the duration of that behavior.

2.3.5.2 Local Field Potential Data

LFP data were extracted for trials of each behavior and inspected for data quality. We had previously observed in early testing of the Neurologger that, due to its fixed amplification settings, data traces could sometimes hit the upper or lower bounds of the visualization range and become clipped at these bounds. Therefore, as a pre-determined criterion for data inclusion, only those trials whose data were contained within the visualization range were used in the following analyses. The total number of trials excluded for mating (ordered by ID) were 31, 16, 0, 4, 19, 6, 11, 10, 44, 4, 0, 16, 1, 4 and 17 (median of 18.8% of original number of mating trials). The total number of trials excluded for self-grooming were 19, 8, 35, 32, 39, 9, 21, 22, 23, 36, 41, 30, 70, 28 and 67 (median of 40.0% of original number of self-grooming trials). The total number of

trials excluded for huddling were 2, 1, 4, 4, 6, 2, 0, 0, 2, 0, 5, 0, 0, 0 and 2 (median of 4.0% of original number of huddling trials). Further, subject 7 had a brief, 12.7-second disruption in data recording and so this data segment was excluded from LFP analyses.

Coherence, Granger causality and cross-frequency coupling were computed between brain regions. All analyses were done in MATLAB unless otherwise noted.

2.3.5.2.1 Coherence

Coherence analyses were performed using multitaper methods (Mitra and Pesaran, 1999) implemented in Chronux (http://chronux.org) (Mitra and Bokil, 2008). This consisted of multiplying each data segment by a set of orthogonal Slepian tapers (Slepian and Pollack, 1961) that specify a spectral concentration bandwidth (± W). W and the segment duration (T) constrain the maximum number of effectively-concentrating tapers to be less than or equal to 2TW-1. Parameters used here were W = 2 Hz, T = 1 second, and 3 tapers. Coherence was then calculated as the magnitude of the coherency, defined in Equation 2 as:

$$C = \frac{S_{12}}{\sqrt{S_{11}S_{22}}} \quad (2)$$

where S_{12} is the cross-spectrum, and S_{11} and S_{22} are the individual power spectra of the two brain regions. S_{12}, S_{11} and S_{22} are averaged over tapers and data trials, as applicable (methodology described further in Jutras et al. (2009)). Coherence ranges from 0 to 1, where a value of 1 represents a perfectly consistent phase and amplitude relationship across tapers and trials.

Coherence estimates were sampled at 1-Hz resolution from 3 Hz to 242 Hz (Subject 3) or 3 Hz to 97 Hz (remaining subjects). This range represents the nearest integer above W that is consistent across subjects to the nearest integer below the (Nyquist frequency - W).

Inter-behavior comparisons: Coherence was compared between 5-s trials of mating, self-grooming and huddling (number of trials listed in section 2.3.5.1.1). To address the possibility of non-stationarity in the data, each trial was split into 40, 1-second segments stepped by 0.1 seconds. Coherence was calculated across trials for each time segment, giving 40 estimates for a given behavior. These estimates were transformed and bias-corrected, as described in section 2.3.6 *Statistics*. They were then averaged to give full-trial estimates of a given behavior. Statistical testing was performed on these averages. In addition, the 2.5 to 97.5 percentile range of the 40 estimates was extracted as a measure of variability (*prctile* function in MATLAB).

2.3.5.2.2 Cross-Frequency Coupling

Cross-frequency coupling was computed using the Modulation Index (MI) metric developed by Tort et al. (2010) (code courtesy of Dr. Adriano Tort and Dr. Teresa Madsen). The MI quantifies the extent to which low-frequency phase of one signal modulates higher-frequency amplitude of another. Briefly, the two signals are filtered in low and high-frequency bands and then Hilbert transformed to obtain the phase and amplitude envelope, respectively. This gives matched phase and amplitude values that are then binned into 20° phase bins. Amplitudes are averaged within each phase bin, giving a distribution of amplitudes over phase bins. This distribution is normalized to the sum of averaged amplitudes. The MI is computed as the normalized Kullback-Leibler distance of this distribution from a uniform (flat/unmodulated) distribution.

The MI was computed over the course of the experiment for each subject ("MI raster"). The baseline and cohabitation periods were broken into 5-s or 2-s non-overlapping time segments. 5-s segments were used to analyze the spectrum of the MI, and 2-s segments were used to relate the MI to behavior (see below). The MI was computed on each segment in two directions: 1) mPFC low-frequency phase modulating NAcc (or off-target) gamma amplitude and 2) NAcc (or off-target) low-frequency phase

modulating mPFC gamma amplitude. This consisted of switching which signals were low- or high-frequency filtered (filtering done using EEGLab package for MATLAB (Delorme and Makeig, 2004), *eegfilt* function).

5-s time segments (MI spectrum): MI was computed at multiple combinations of phase and amplitude frequencies. Phase frequencies ranged from 3 to 21 Hz, with integer spacing and bandwidth ± 0.5 Hz. Amplitude frequencies ranged from 32 to 84 Hz, with spacing of 4 Hz and bandwidth ± 2 Hz. To measure the relative strength of MI in the mPFC-to-NAcc direction ("net modulation") at a given phase/amplitude frequency combination, the MI computed for the NAcc-to-mPFC direction was subtracted from that of the mPFC-to-NAcc direction. The net modulation was averaged across all time segments and hit animals to identify the frequency combination producing maximal net modulation. The same analysis was performed on non-hit animals.

2-s time segments (MI and behavior): Net modulation was computed at a phase frequency of 5 Hz and amplitude frequency of 80 Hz. These time segments were matched to raster time samples coded as specific behaviors (see section 2.3.5.1.2) and averaged across values coded as the same behavior to estimate the net modulation during that behavior. Averages were taken over the full cohabitation as well as shorter time segments (e.g. within first or last mating bout).

2.3.5.2.3 Granger Causality

Granger causality was computed with parametric methods (Brovelli et al., 2004; Dhamala, 2014) implemented in code by Dr. Stijn de Waele and Dr. Nathan J. Killian and adapted to use by Varun Saravanan and Elizabeth Amadei. Granger causality tests the degree to which previous values of one time series improve the prediction of a different time series (Granger, 1969) and was used here to assess the directional influence of one brain area over another's activity (Gregoriou et al., 2009) during mating. Granger causality can be formulated in the frequency domain by fitting and frequency-

transforming a bivariate autoregressive model to the two time series (Brovelli et al., 2004) (here, mPFC and NAcc LFPs during mating). The power of each time series can then be estimated and decomposed into an intrinsic component and a causal component contributed by the other time series. Granger causality is computed as the natural log of the ratio of the total power (intrinsic + causal) to the intrinsic power.

To fit the autoregressive model, the average values of the time series were subtracted out to produce means of 0 and model parameters estimated using the Nuttall-Strand method. The model order was selected using the Combined Information Criterion (de Waele and Broersen, 2003).

Granger causality was compared in the mPFC-to-NAcc and NAcc-to-mPFC directions during mating (see section 2.3.6 *Statistics*). As in the coherence and power estimates, 5-second trials of mating were split into 40, 1-second segments shifted by 0.1 seconds. Granger causality was computed on each segment (see below) at integer frequencies from 0 Hz to 244 Hz (Subject 3) or to 99 Hz (all other subjects), and then averaged over segments to get a full-trial estimate. The 2.5 to 97.5 percentile range of the 40 estimates was extracted as a measure of variability. The upper bound of the frequency range represents the nearest integer below the Nyquist frequency.

Granger causality was calculated using a bootstrapping procedure. Briefly, for a subject with *n* trials of mating, *n* segments matched in time were extracted from the trials. 1000 artificial sets of *n* segments were generated by randomly selecting with replacement from possible segments. Autoregressive model parameters were averaged across segments in each set, and these average values used to compute Granger causality in the two directions. The actual Granger causality values were defined as the mean over all sets.

2.3.6 Statistics

Statistical tests used a significance level (α) of 0.05 (* $P < 0.05$, ** $P < 0.01$, *** $P < 0.001$). Statistical analyses were performed separately on hit ($n = 9$) and non-hit ($n = 6$) groups.

Correlation analyses used the Pearson correlation (*corr* in MATLAB) and report R^2 and *P*-values. Linear regression was performed using the function *polyfit* in MATLAB.

In tests of paired samples, a two-sided Lilliefors test (*lillietest* in MATLAB) was used to test the normality of the difference between samples. This test was also used to test the normality of individual groups for ANOVAs. Since this test is less sensitive to small sample sizes, data were also visually inspected for any obvious skew. Parametric (*t*- and ANOVA) tests were used when justified by these analyses.

The Bonferroni method was used to correct for multiple comparisons. The number of corrections and other figure-specific statistical methods are described below. *P*-values are uncorrected unless otherwise specified.

Figure 2.2: To compare mPFC-NAcc coherence between mating, self-grooming and huddling, the 40 within-trial coherence estimates for each of these behaviors were first Fisher-transformed. They were then bias-corrected for different sample sizes (here: number of trials of each behavior), as described in Bokil et al. (2007). Upon averaging these 40 estimates to get a full-trial estimate, the peak frequency of mating coherence was determined for each subject (ranged from 4 to 6 Hz), and the mode of these frequencies across subjects (5 Hz) was used for inter-subject comparisons. The effect of behavior on coherence was tested using a one-way repeated measures ANOVA with behavior as the within-subject factor (SPSS). Sphericity was verified using Mauchly's Test (SPSS, $W = 0.60$, $P = 0.167$). The difference in coherence between 1) mating and self-grooming, 2) mating and huddling coherence and 3) self-grooming and huddling at 5 Hz was tested for significance using a post hoc two-tailed paired *t*-test (*ttest* in MATLAB), with correction for 3 comparisons.

The same analysis was performed on non-hit animals, with coherence evaluated at 5 Hz. Sphericity was verified using Mauchly's Test (W = 0.62, P = 0.380).

Figure 2.3: The number of bouts, duration and latency of mating, self-grooming and huddling were compared between hit and non-hit groups using Wilcoxon signed-rank tests (*signrank* in MATLAB). P-values were corrected for 9 comparisons.

The effect of behavior on latency was tested using a Friedman Test due to violations of normality. The difference in latency between 1) mating and self-grooming, 2) mating and huddling and 3) self-grooming and huddling was tested for significance using a post hoc Wilcoxon signed-rank test, with correction for 3 comparisons.

Correlations between huddling latency and mating and self-grooming duration and latency parameters were corrected for 8 comparisons.

Figure 2.4: The effect of behavior (huddling, baseline, nonhuddling) on mPFC-NAcc net modulation was tested using a one-way repeated measures ANOVA with behavior as the within-subject factor (SPSS). Sphericity was violated (Mauchly's Test; W = 0.36, P = 0.028) and so the Greenhouse-Geisser correction was applied. The difference in net modulation between 1) nonhuddling and huddling, 2) nonhuddling and baseline and 3) huddling and baseline was tested for significance using a post hoc two-tailed paired t-test (*ttest* in MATLAB), with correction for 3 comparisons. The same ANOVA analysis was performed on non-hit animals, with Greenhouse-Geisser correction applied due to violation of sphericity (Mauchly's Test; W = 0.05, P = 0.003).

Pairwise correlations between net modulation during specific behaviors (mating, self-grooming, non-coded) were corrected for 3 comparisons.

Figure 2.6: To compare Granger causality in the mPFC-to-NAcc and NAcc-to-mPFC directions, Granger causality values in each direction were obtained for each subject at 5 Hz, the same frequency used in coherence comparisons. The difference of

the two directions (mPFC-to-NAcc - NAcc-to-mPFC) across subjects was tested for significance using a two-tailed paired *t*-test.

Figure 2.7: Net modulation during mating, self-grooming and non-coded behaviors were compared to each other using Wilcoxon signed-rank tests.

Figure 2.9: Correlations between huddling latency and net modulation during mating, self-grooming and non-coded behaviors were corrected for 3 comparisons.

Correlations between huddling latency and nonhuddling net modulation during the baseline period, first 60 minutes of cohabitation and full cohabitation were corrected for 3 comparisons.

A permutation test was used to test whether the correlation between huddling latency and nonhuddling net modulation significantly improved from before to after mating. The before time point was that immediately before mating. The after time point was that which produced the highest correlation between net modulation and huddling latency within 2.5 min after mating (see Figure 2.9o,q; bracket indicates before and after points). Briefly, for each time point (before or after), net modulation values were randomized across subjects (using *datasample* in MATLAB) and then correlated with the huddling latency (kept in subject order). The difference in R^2 (abs. value) between these correlations was then computed. This re-sampling procedure was repeated $1x10^6$ times to produce a permuted (null) distribution of R^2 differences. A two-sided *P*-value was obtained as the proportion of shuffled R^2 differences that were greater than the observed value.

Figure 2.10: To calculate the mean net modulation during early and late mating for each subject, net modulation values coded as mating were taken from that subject's first and last mating bouts, respectively, and then averaged. The number of values within the first bout were (in subject order): 19, 41, 38, 25, 62, 24, 22, 101, 84, 36, 20, 22, 10, 21 and 31. The number of values within the last bout were (in subject order): 48, 52, 24,

26, 70, 34, 35, 57, 38, 45, 33, 33, 20, 24 and 25. To calculate the mean net modulation during early and late self-grooming for each subject, net modulation values coded as self-grooming were taken from that subject's start (moving forward) or end (moving backward) of the cohabitation. The number of self-grooming values were matched to that subject's first and last mating bout (listed above), respectively. The difference of early and late mean net modulation for each behavior across subjects was performed using a Wilcoxon signed-rank test and Bonferroni-corrected for 2 comparisons.

Figure 2.11: The same permutation test described for Figure 2.9 was used to test whether the correlation between huddling latency and nonhuddling net modulation significantly improved from before to after self-grooming.

Figure 2.12: In optogenetics analyses, the relative time spent with the partner in the PPT (partner time minus stranger time) was compared between treatment (expressing ChR2) and control (expressing control fluorophore lacking ChR2) groups using a permutation test. This test was chosen due to normality violations in group and residual values (discouraging an ANOVA approach). The permutation test involved calculating the effect size (Cohen's *d* (Cohen, 1992) (abs. value)) of the difference between treatment and control groups in the relative time spent with the partner. This observed Cohen's *d* was then compared to a permuted distribution of Cohen's *d* values created by randomly assigning data values without replacement to treatment and control groups (using *randperm* in MATLAB). The re-sampling procedure was performed $1x10^6$ times. A two-sided *P*-value was obtained as the proportion of shuffled Cohen's *d* values that were greater than the observed value.

The same permutation approach was used to compare the total duration of optical stimulation as well as time spent in the social, neutral and non-social zones (see Figure 2.1d) during cohabitation between treatment and control groups. Due to a brief power outage after the optical stimulation period for one control animal, video and

tracking data for that subject was lost even though it received normal stimulation. Therefore, the number of control subjects used in the optical stimulation and zone analyses is one less than that used in the PPT analyses described above (n = 10 as opposed to 11).

2.4 Collaborator Contributions

The main collaborators on this work were Dr. Zachary V. Johnson (Z.V.J.), Yong Jun Kwon (Y.K.), Aaron C. Shpiner (A.C.S.), Varun Saravanan (V.S.), Wittney D. Mays (W.D.M.), Dr. Steven J. Ryan (S.J.R.), Dr. Hasse Walum (H.W.), Dr. Donald G. Rainnie (D.G.R.), Dr. Larry J. Young (L.J.Y.) and Dr. Robert C. Liu (R.C.L.). My and each collaborator's contributions are summarized below. I adapted the Neurologger to a vole preparation and designed and performed *in vivo* electrophysiology experiments, which motivated an optogenetics approach; optogenetics experiments were designed and performed by Z.V.J. and me, assisted by Y.K.; Z.V.J. validated viral techniques and performed optogenetics surgeries and histology; S.J.R. and I designed slice electrophysiology experiments; Z.V.J. performed all surgeries and histology for slice electrophysiology experiments; S.J.R. performed slice electrophysiology experiments, supervised and assisted by D.G.R. and me, respectively; I, Z.V.J., Y.K., S.J.R., H.W., A.C.S., V.S. and W.D.M. analyzed data; I drafted the manuscript of this work (citation in footnote on page 13); Z.V.J., A.C.S., Y.K., S.J.R., H.W. and V.S. contributed to the writing; R.C.L. and L.J.Y. edited the manuscript and supervised all aspects of this work.

CHAPTER 3

DISCUSSION AND FUTURE DIRECTIONS

Previous studies in prairie voles have identified the mPFC and NAcc as important for bond formation (Johnson and Young, 2015; McGraw and Young, 2010; Young and Wang, 2004), but how these brain areas are dynamically activated during social interactions leading to a bond has been unknown. In this thesis, I addressed this gap by performing detailed behavioral scoring, electrophysiological (LFP) recording and optogenetic manipulation in freely-behaving, socially-interacting female voles. LFP recordings revealed elevated low-frequency (<10 Hz) coherence, a measure of functional connectivity, between mPFC and NAcc during mating, a behavior that accelerates bond formation (Williams et al., 1992). This enhancement was also observed in a second (control) group of animals with electrodes targeting the mPFC and BNST, indicating that mating elevates low-frequency connectivity across multiple brain areas.

I then examined how low-frequency mPFC-NAcc connectivity modulates local activity in each area using a cross-frequency coupling analysis ("net modulation"). A key finding was that individual subjects varied in the strength of their net modulation. This could not be explained by individual variability in the exact electrode placement within mPFC and NAcc nor the amount or timing of mating and self-grooming – behaviors during which individual variability in the net modulation was most prominent. Instead, net modulation within the mPFC-NAcc, but not the mPFC-BNST, circuit correlated with animals' latency to begin huddling, a key affiliative behavior that emerges over the course of cohabitation.

Additional analyses showed that the correlation between mPFC-NAcc net modulation and huddling latency emerged over time, largely coinciding with the timing of

the first mating bout. This led me to focus on the change in net modulation from before to after mating, which I found to predict both subsequent net modulation over a sustained post-mating period as well as the latency to huddle triggered from the end of the mating bout. Indeed, the correlation between net modulation and huddling latency improved from immediately before to after mating. Together, these results indicate that the mPFC-NAcc circuit is recruited during social bond formation and that individual variability in its activation, particularly after the first mating event, relates to how quickly animals become affiliative.

These electrophysiological results raised the possibility that stimulating the mPFC-NAcc circuit could accelerate the emergence of affiliative behavior. To test this, I optogenetically stimulated mPFC afferents in the NAcc during a restricted cohabitation paradigm without mating, which would normally not produce a social bond, as measured by the PPT. Optical stimulation was delivered at the same low-frequencies (5-6 Hz) at which I previously observed enhanced coherence and net modulation. A control group lacking the excitatory opsin was used to control for light delivery and experience in the experimental cage. When tested on the PPT the following day, treatment animals spent significantly greater relative time huddling with their partner versus the stranger, indicating that mPFC-NAcc circuit activation increased animals' preference towards the partner. Together, these electrophysiological and optogenetic results are consistent with the hypothesis that the mPFC-NAcc circuit becomes activated during social experience with a partner to switch animals towards increased affiliation.

These results raise three conceptual implications for future research that will be discussed below. These are the functions of 1) neurochemicals OT and DA in modulating mPFC-NAcc functional connectivity, 2) mPFC drive to NAcc in modulating NAcc spiking activity and plasticity in a social learning context, and 3) other brain circuits in vole bond formation.

3.1 OT and DA Modulation of mPFC-NAcc Functional Connectivity

Previous pharmacological and genetic manipulation studies in voles have implicated the central action of OT and DA, particularly within the NAcc, in facilitating bond formation. For example, central OT infusion (Williams et al., 1994) and upregulation of NAcc OTR (Ross et al., 2009b) accelerates bond formation, as does infusion of a D2R agonist into the NAcc (Gingrich et al., 2000). However, these approaches provide a static picture of OT and DA activation in mPFC and NAcc and are not technically suited to measuring the dynamic activity of these brain areas during natural social interactions. Given that bond formation requires a shift towards increasing affiliation and that, within this thesis, I demonstrate that the strength of mPFC's modulation of NAcc activity correlates with how quickly animals become affiliative, one hypothesis is that OT and/or DA increase the strength of mPFC-NAcc functional connectivity to accelerate vole bond formation.

This hypothesis could be examined by combining electrophysiological recording with manipulations of neurochemical systems in socially-interacting animals. For example, neurochemical action could be blocked in mPFC and/or NAcc using site-specific infusion of an OTR or D2R antagonist (Gingrich et al., 2000; Young et al., 2001) or shRNA downregulation of neurochemical receptors (Keebaugh et al., 2015). In complement, neurochemical action could be enhanced by infusing the neurochemical (e.g. OT (Williams et al., 1994)) or its agonist (e.g. D2 agonist (Gingrich et al., 2000)) as well as upregulating neurochemical receptor expression in individual brain areas (Ross et al., 2009b). Whether 1) neurochemical inhibition during cohabitation delays affiliative behavior and reduces mPFC-NAcc functional connectivity and/or 2) neurochemical enhancement accelerates affiliative behavior and increases mPFC-NAcc functional connectivity could both be tested. The delay or acceleration of affiliative behavior could be assayed using the cohabitation "huddling latency" metric included in this thesis. This

would capture the emergence of affiliative behavior during bond formation. Additionally, it could be validated against a subsequent PPT, which was not performed in this thesis for simplicity but is the traditional metric for assessing bond formation performed after cohabitation (Ahern et al., 2009). It would be useful to compare both metrics to determine their consistency and relationship to brain activity.

Inter-subject variability in neurochemical receptor expression is another avenue for investigating the influence of neurochemicals on mPFC-NAcc circuit activation. There is substantial inter-subject variability in NAcc OTR expression that has previously been associated with maternal behavior and pair bonding in prairie voles (Barrett et al., 2015; King et al., 2016; Olazábal and Young, 2006). For example, Olazábal and Young (2006) showed greater maternal behavior (e.g. licking, grooming and hovering over pups) in females with high NAcc OTR expression. King et al. (2016) discovered a single nucleotide polymorphism within the OTR gene that predicted NAcc OTR expression and partner preference formation in males. Barrett et al. (2015) exposed females to early life isolation and found that individuals' NAcc OTR expression correlated with the strength of their partner preferences in adulthood, a measure of resiliency to early life stress. These studies raise the possibility that individual variation in NAcc OTR expression and/or OTR genotype correlates with mPFC-NAcc functional connectivity, which can be tested in future studies by combining electrophysiology with standard autoradiography and genotyping approaches. Such a study would be scientifically significant in potentially linking individual variability across the dimensions of anatomy or genotype, brain activity and behavior.

3.2 mPFC Modulation of NAcc Spiking Activity and Plasticity

This thesis uses LFP gamma activity as a measure of local network activation (Buzsáki and Wang, 2012) and finds that mPFC low-frequency (~5 Hz) oscillations directionally modulate gamma (~80 Hz) activity within NAcc (net modulation). A key

question is how the various NAcc cell types fire relative to the gamma rhythm. Striatal FSIs and MSNs can phase-entrain their firing to LFP gamma in behaving rats (Berke, 2009; Kalenscher et al., 2010), raising the possibility that mPFC rhythmically modulates the excitability of multiple cell types during vole bonding. Indeed, brief high-frequency (bursting) mPFC stimulation in anesthetized rats both depolarizes MSNs and increases the firing of FSIs (Gruber and O'Donnell, 2009; Gruber et al., 2009b). During mPFC stimulation, MSNs are also inhibited due to local network interactions, which can refine (even prevent) their firing despite being depolarized (Gruber et al., 2009b).

How mPFC modulates the firing of NAcc cell types and their interactions during social reward and learning remains an open question of scientific interest. For example, Kalenscher et al. (2010) recorded LFPs and spiking activity from the NAcc of rats running on a triangular task to obtain food or liquid rewards that were baited at three locations. A subset of units, termed “task-related”, altered their firing rate during or before animals’ reward site visits. Compared to non-task-related units, a greater proportion of task-related units phase-locked their firing to a LFP gamma oscillation measured during the task. Whether a similar population of neurons are activated during social interactions in voles and alter their firing relative to social reward (e.g. before or during mating) could be examined by electrophysiological recording of spiking activity in socially-interacting voles. Further, a role for mPFC in modulating NAcc unit entrainment to gamma oscillations could be investigating by combining electrophysiological recording with optogenetic stimulation of mPFC afferents.

In testing the local effects of mPFC input, it would be particularly relevant to examine its frequency-dependence. Both this thesis and previous work (summarized in introduction (Bagot et al., 2015; Britt et al., 2012; Gruber et al., 2009a)) appear to converge on low frequency (<10 Hz) mPFC drive as being functionally relevant for motivated behavior and behavioral switching. How specific this frequency is in exerting

such behavioral effects and why it does so, in terms of the activity of NAcc cell types, their interactions, and/or synaptic plasticity during behavior, remains unclear. Interestingly, Berke (2009) identified FSIs that entrain their firing to both high-gamma (~80 Hz) and low-frequency (~8 Hz) oscillations, raising the possibility that low-frequency mPFC drive is ideally suited to recruiting local NAcc populations. Whether altering the frequency of mPFC drive to NAcc in a vole bonding paradigm (e.g. by varying the optogenetic stimulation frequency of mPFC afferents in NAcc) disrupts the entrainment of NAcc neurons as well as subsequent affiliative behavior could be tested.

A related question is whether mPFC drive to NAcc during bond formation mediates local plasticity within the NAcc. The NAcc has been proposed to consist of functionally-distinct neuronal ensembles that are activated by specific cues and contexts and bias the resulting selection of behaviors (Floresco, 2015; Pennartz et al., 1994). Ensemble representations can be acquired through experience. For example, Cruz et al. (2014) tested whether an ensemble representation existed for a context paired with cocaine delivery. Rats were trained to self-infuse cocaine within a given context (A). This behavior was then extinguished in a second context (B). Rats were then re-exposed to the A or a novel context (C), and the Daun02 inactivation method (Koya et al., 2009) used to label and inactivate neurons activated by this exposure. While neuronal inactivation was still in effect, animals were re-exposed to A to test for reinstatement of drug seeking. The exposure to context A versus C enabled the experimenters to test whether inactivating the specific population of neurons associated with context A disrupted animals' drug seeking behavior in that same context. Indeed, only animals whose context A-associated neurons were inactivated showed disrupted reinstatement compared to vehicle-infused animals, suggesting that the drug-paired context and its associated behavioral response were encoded by a specific ensemble of NAcc neurons.

This study motivates the hypothesis that, over the course of vole bond formation, the partner and associated affiliative behavior towards the partner acquire an ensemble representation within the NAcc. Transgenic approaches are still being adapted to the prairie vole, and so the Daun02 inactivation method and other re-activation methods (e.g. fos:tTA/TRE (Liu et al., 2012; Okuyama et al., 2016)) are not yet feasible in voles. However, an IEG approach in which cells are co-labeled for two members of the Fos family of transcription factors, the IEG c-Fos and the IEG product ΔFOSB (Conversi et al., 2008; Cruz et al., 2013; Mattson et al., 2008), could be a first step to investigate this question. In this approach, repeated neural activation such as which occurs across learning trials (e.g. repeated cocaine-context pairings to induce locomotor sensitization (Mattson et al., 2008)), causes ΔFOSB to be expressed and accumulate in cells. An acute testing session (e.g. single exposure to the drug paired context) causes c-Fos to be activated, which is then co-labeled with ΔFOSB using *in situ* hybridization and immunohistochemistry, respectively. Co-labeling has been used to identify neurons activated during locomotor sensitization to a cocaine-paired context (Mattson et al., 2008). A similar approach could be attempted in voles to identify neurons activated by a bonded partner. This would involve quantifying ΔFOSB from bond formation (either from one cohabitation or multiple cohabitation "sessions") and c-Fos from the PPT. The amount of co-labeling could then be related to animals' performance on the PPT, with the hypothesis that animals with stronger partner preferences show greater ΔFOSB/c-Fos co-labeling, suggesting a neuronal ensemble encoding the partner. The role of the mPFC could be examined through low-frequency optogenetic stimulation of mPFC afferents in the NAcc during cohabitation, shown in this thesis to shift animals' preference towards the partner in the PPT.

3.3 Other Brain Circuits Converging in NAcc

In addition to mPFC input, the NAcc also receives glutamatergic afferents from the hippocampus (Phillipson and Griffiths, 1985), which may also be recruited during vole bond formation. For example, Okuyama et al. (2016) implicated ventral hippocampal projections to the NAcc shell in social recognition memory. Specifically, they familiarized mice to a conspecific and then tested their recognition memory in a social discrimination test, in which each freely-moving subject was exposed to the familiarized conspecific as well as a novel conspecific (restrained under cups). Mice typically spend more time interacting with a novel conspecific, and so the relative amount of time spent close to the familiarized versus novel animal was quantified as a measure of social memory. As expected, control animals with intact ventral hippocampal-NAcc connectivity spent significantly longer with the novel animal compared to the familiar. However, optogenetic inhibition of the ventral hippocampal-NAcc circuit in the full cage or specifically during interaction with the familiar animal abolished the preference for the novel animal. This result was specific to the social discrimination test, as circuit inhibition did not disrupt preference for novel objects or contexts. How this circuit may be activated during vole bond formation to promote a memory for the partner could be investigated using electrophysiological recording and optogenetic manipulations.

The BLA provides an additional glutamatergic input to NAcc (Phillipson and Griffiths, 1985). This circuit has been implicated in the expression of cue-evoked motivated behaviors (Janak and Tye, 2015). For example, Stuber et al. (2011) found that optogenetic inhibition of BLA afferents in the NAcc of mice disrupted cue-evoked licking behavior for sucrose. Ambroggi et al. (2008) further showed that pharmacological inactivation of BLA in rats disrupted tone-evoked lever pressing for sucrose as well as cue-evoked firing in NAcc. Whether the BLA-NAcc circuit is necessary for the expression

of affiliative behavior in pair bonded voles could be tested using optogenetic or pharmacological inactivation.

In summary, my studies exploit an ethologically-relevant paradigm (vole bond formation) to reveal dynamic neurobiological processes underlying natural social behavior. These studies in the vole system now open the door to exciting future investigations to better understand the brain circuits and mechanisms that support complex prosocial behaviors as they naturally unfold through social interactions.

REFERENCES

Acevedo, B.P., Aron, A., Fisher, H.E., and Brown, L.L. (2011). Neural correlates of long-term intense romantic love. Soc Cogn Affect Neurosci *7*, 145-159.

Adinoff, B. (2004). Neurobiologic processes in drug reward and addiction. Harv Rev Psychiatry *12*, 305-320.

Ahern, T.H., Modi, M.E., Burkett, J.P., and Young, L.J. (2009). Evaluation of two automated metrics for analyzing partner preference tests. J Neurosci Methods *182*, 180-188.

Ambroggi, F., Ishikawa, A., Fields, H.L., and Nicola, S.M. (2008). Basolateral amygdala neurons facilitate reward-seeking behavior by exciting nucleus accumbens neurons. Neuron *59*, 648-661.

Aragona, B.J., Liu, Y., Yu, Y.J., Curtis, J.T., Detwiler, J.M., Insel, T.R., and Wang, Z. (2006). Nucleus accumbens dopamine differentially mediates the formation and maintenance of monogamous pair bonds. Nat Neurosci *9*, 133-139.

Bagot, R.C., Parise, E.M., Pena, C.J., Zhang, H.-X., Maze, I., Chaudhury, D., Persaud, B., Cachope, R., Bolanos-Guzman, C.A., Cheer, J.F.*, et al.* (2015). Ventral hippocampal afferents to the nucleus accumbens regulate susceptibility to depression. Nat Commun *6*, 7062.

Barrett, C.E., Arambula, S.E., and Young, L.J. (2015). The oxytocin system promotes resilience to the effects of neonatal isolation on adult social attachment in female prairie voles. Transl Psychiatry *5*, e606.

Bartels, A., and Zeki, S. (2000). The neural basis of romantic love. Neuroreport *11*, 3829-3834.

Berens, P., Keliris, G.A., Ecker, A.S., Logothetis, N.K., and Tolias, A.S. (2008). Feature selectivity of the gamma-band of the local field potential in primate primary visual cortex. Front Neurosci *2*, 199-207.

Berke, J.D. (2009). Fast oscillations in cortical-striatal networks switch frequency following rewarding events and stimulant drugs. Eur J Neurosci *30*, 848-859.

Block, A.E., Dhanji, H., Thompson-Tardif, S.F., and Floresco, S.B. (2007). Thalamic–prefrontal cortical–ventral striatal circuitry mediates dissociable components of strategy set shifting. Cereb Cortex *17*, 1625-1636.

Bokil, H., Purpura, K., Schoffelen, J.-M., Thomson, D., and Mitra, P. (2007). Comparing spectra and coherences for groups of unequal size. J Neurosci Methods *159*, 337-345.

Bossert, J.M., Stern, A.L., Theberge, F.R., Marchant, N.J., Wang, H.L., Morales, M., and Shaham, Y. (2012). Role of projections from ventral medial prefrontal cortex to nucleus

accumbens shell in context-induced reinstatement of heroin seeking. J Neurosci *32*, 4982-4991.

Britt, J.P., Benaliouad, F., McDevitt, R.A., Stuber, G.D., Wise, R.A., and Bonci, A. (2012). Synaptic and behavioral profile of multiple glutamatergic inputs to the nucleus accumbens. Neuron *76*, 790-803.

Brog, J.S., Salyapongse, A., Deutch, A.Y., and Zahm, D.S. (1993). The patterns of afferent innervation of the core and shell in the “accumbens” part of the rat ventral striatum: Immunohistochemical detection of retrogradely transported fluoro-gold. J Comp Neurol *338*, 255-278.

Brovelli, A., Ding, M., Ledberg, A., Chen, Y., Nakamura, R., and Bressler, S.L. (2004). Beta oscillations in a large-scale sensorimotor cortical network: directional influences revealed by Granger causality. Proc Natl Acad Sci USA *101*, 9849-9854.

Buzsáki, G., and Wang, X.-J. (2012). Mechanisms of gamma oscillations. Annu Rev Neurosci *35*, 203-225.

Chang, H.T., and Kitai, S.T. (1985). Projection neurons of the nucleus accumbens: an intracellular labeling study. Brain Res *347*, 112-116.

Cho, M.M., DeVries, A.C., Williams, J.R., and Carter, C.S. (1999). The effects of oxytocin and vasopressin on partner preferences in male and female prairie voles (Microtus ochrogaster). Behav Neurosci *113*, 1071-1079.

Christie, M.J., Summers, R.J., Stephenson, J.A., Cook, C.J., and Beart, P.M. (1987). Excitatory amino acid projections to the nucleus accumbens septi in the rat: a retrograde transport study utilizing D[3H]aspartate and [3H]GABA. Neuroscience *22*, 425-439.

Cohen, J. (1992). A power primer. Psychol Bull *112*, 155-159.

Conversi, D., Bonito-Oliva, A., Orsini, C., Colelli, V., and Cabib, S. (2008). DeltaFosB accumulation in ventro-medial caudate underlies the induction but not the expression of behavioral sensitization by both repeated amphetamine and stress. Eur J Neurosci *27*, 191-201.

Cruz, F.C., Babin, K.R., Leao, R.M., Goldart, E.M., Bossert, J.M., Shaham, Y., and Hope, B.T. (2014). Role of nucleus accumbens shell neuronal ensembles in context-induced reinstatement of cocaine-seeking. J Neurosci *34*, 7437-7446.

Cruz, F.C., Koya, E., Guez-Barber, D.H., Bossert, J.M., Lupica, C.R., Shaham, Y., and Hope, B.T. (2013). New technologies for examining the role of neuronal ensembles in drug addiction and fear. Nat Rev Neurosci *14*, 743-754.

Damsma, G., Pfaus, J.G., Wenkstern, D., Phillips, A.G., and Fibiger, H.C. (1992). Sexual behavior increases dopamine transmission in the nucleus accumbens and striatum of male rats: Comparison with novelty and locomotion. Behav Neurosci *106*, 181-191.

de Waele, S., and Broersen, M.T. (2003). Order selection for vector autoregressive models. IEEE T Signal Proces *51*, 427-433.

Delorme, A., and Makeig, S. (2004). EEGLAB: an open source toolbox for analysis of single-trial EEG dynamics including independent component analysis. J Neurosci Methods *134*, 9-21.

Dhamala, M. (2014). Spectral Interdependency Methods. In Encyclopedia of Computational Neuroscience, D. Jaeger, and R. Jung, eds. (New York: Springer), pp. 2789-2793.

Donaldson, Z.R., Spiegel, L., and Young, L.J. (2010). Central vasopressin V1a receptor activation is independently necessary for both partner preference formation and expression in socially monogamous male prairie voles. Behav Neurosci *124*, 159-163.

Etholm, L., Arabadzisz, D., Lipp, H.P., and Heggelund, P. (2010). Seizure logging: a new approach to synchronized cable-free EEG and video recordings of seizure activity in mice. J Neurosci Methods *192*, 254-260.

Floresco, S.B. (2015). The nucleus accumbens: an interface between cognition, emotion, and action. Annu Rev Psychol *66*, 25-52.

Getz, L.L., Carter, C.S., and Gavish, L. (1981). The mating system of the prairie vole, Microtus-ochrogaster: field and laboratory evidence for pair-bonding. Behav Ecol Sociobiol *8*, 189-194.

Ghods-Sharifi, S., and Floresco, S.B. (2010). Differential effects on effort discounting induced by inactivations of the nucleus accumbens core or shell. Behav Neurosci *124*, 179-191.

Gingrich, B., Liu, Y., Cascio, C., Wang, Z., and Insel, T.R. (2000). Dopamine D2 receptors in the nucleus accumbens are important for social attachment in female prairie voles (Microtus ochrogaster). Behav Neurosci *114*, 173-183.

Gorelova, N., and Yang, C.R. (1996). The course of neural projection from the prefrontal cortex to the nucleus accumbens in the rat. Neuroscience *76*, 689-706.

Granger, C.W.J. (1969). Investigating causal relations by econometric models and cross-spectral methods. Econometrica *37*, 424-438.

Gregoriou, G.G., Gotts, S.J., Zhou, H., and Desimone, R. (2009). High-frequency, long-range coupling between prefrontal and visual cortex during attention. Science *324*, 1207-1210.

Gruber, A.J., Hussain, R.J., and O'Donnell, P. (2009a). The nucleus accumbens: a switchboard for goal-directed behaviors. PLoS ONE *4*, e5062.

Gruber, A.J., and O'Donnell, P. (2009). Bursting activation of prefrontal cortex drives sustained up states in nucleus accumbens spiny neurons in vivo. Synapse *63*, 173-180.

Gruber, A.J., Powell, E.M., and O'Donnell, P. (2009b). Cortically activated interneurons shape spatial aspects of cortico-accumbens processing. J Neurophysiol *101*, 1876-1882.

Gutman, D.A., Keifer Jr, O.P., Magnuson, M.E., Choi, D.C., Majeed, W., Keilholz, S., and Ressler, K.J. (2012). A DTI tractography analysis of infralimbic and prelimbic connectivity in the mouse using high-throughput MRI. NeuroImage *63*, 800-811.

Hazan, C., and Shaver, P. (1987). Romantic love conceptualized as an attachment process. J Pers Soc Psychol *52*, 511-524.

Hearing, M.C., Zink, A.N., and Wickman, K. (2012). Cocaine-induced adaptations in metabotropic inhibitory signaling in the mesocorticolimbic system. Rev Neurosci *23*, 325-351.

Heimer, L., Zahm, D.S., Churchill, L., Kalivas, P.W., and Wohltmann, C. (1991). Specificity in the projection patterns of accumbal core and shell in the rat. Neuroscience *41*, 89-125.

Hernandez, L., and Hoebel, B.G. (1988). Food reward and cocaine increase extracellular dopamine in the nucleus accumbens as measured by microdialysis. Life Sci *42*, 1705-1712.

Hoover, W.B., and Vertes, R.P. (2007). Anatomical analysis of afferent projections to the medial prefrontal cortex in the rat. Brain Struct Funct *212*, 149-179.

Insel, T.R., and Hulihan, T.J. (1995). A gender-specific mechanism for pair bonding - oxytocin and partner preference formation in monogamous voles. Behav Neurosci *109*, 782-789.

Insel, T.R., and Shapiro, L.E. (1992). Oxytocin receptor distribution reflects social organization in monogamous and polygamous voles. Proc Natl Acad Sci USA *89*, 5981-5985.

Janak, P.H., and Tye, K.M. (2015). From circuits to behaviour in the amygdala. Nature *517*, 284-292.

Johnson, Z.V., Walum, H., Jamal, Y.A., Xiao, Y., Keebaugh, A.C., Inoue, K., and Young, L.J. (2016). Central oxytocin receptors mediate mating-induced partner preferences and enhance correlated activation across forebrain nuclei in male prairie voles. Horm Behav *79*, 8-17.

Johnson, Z.V., Walum, H., Xiao, Y., Riefkohl, P.C., and Young, L.J. (2017). Oxytocin receptors modulate a social salience neural network in male prairie voles. Horm Behav *87*, 16-24.

Johnson, Z.V., and Young, L.J. (2015). Neurobiological mechanisms of social attachment and pair bonding. Curr Opin Behav Sci *3*, 38-44.

Jutras, M.J., Fries, P., and Buffalo, E.A. (2009). Gamma-band synchronization in the macaque hippocampus and memory formation. J Neurosci *29*, 12521-12531.

Kahn, J.B., Ward, R.D., Kahn, L.W., Rudy, N.M., Kandel, E.R., Balsam, P.D., and Simpson, E.H. (2012). Medial prefrontal lesions in mice impair sustained attention but spare maintenance of information in working memory. Learn Mem *19*, 513-517.

Kalenscher, T., Lansink, C.S., Lankelma, J.V., and Pennartz, C.M.A. (2010). Reward-associated gamma oscillations in ventral striatum are regionally differentiated and modulate local firing activity. J Neurophysiol *103*, 1658-1672.

Keebaugh, A.C., Barrett, C.E., Laprairie, J.L., Jenkins, J.J., and Young, L.J. (2015). RNAi knockdown of oxytocin receptor in the nucleus accumbens inhibits social attachment and parental care in monogamous female prairie voles. Soc Neurosci *10*, 561-570.

Kendrick, K.M. (2000). Oxytocin, motherhood and bonding. Exp Physiol *85*, 111S-124S.

Kendrick, K.M., Keverne, E.B., Baldwin, B.A., and Sharman, D.F. (1986a). Cerebrospinal fluid levels of acetylcholinesterase, monoamines and oxytocin during labour, parturition, vaginocervical stimulation, lamb separation and suckling in sheep. Neuroendocrinology *44*, 149-156.

Kendrick, K.M., Keverne, E.B., Baldwin, B.A., and Sharman, D.F. (1986b). Cerebrospinal fluid levels of acetylcholinesterase, monoamines and oxytocin during labour, parturition, vaginocervical stimulation, lamb separation and suckling in sheep. Neuroendocrinology *44*, 149-156.

King, L.B., Walum, H., Inoue, K., Eyrich, N.W., and Young, L.J. (2016). Variation in the oxytocin receptor gene predicts brain region–specific expression and social attachment. Biol Psychiatry *80*, 160-169.

Kleiman, D.G. (1977). Monogamy in mammals. Q Rev Biol *52*, 39-69.

Koya, E., Golden, S.A., Harvey, B.K., Guez-Barber, D.H., Berkow, A., Simmons, D.E., Bossert, J.M., Nair, S.G., Uejima, J.L., Marin, M.T.*, et al.* (2009). Targeted disruption of cocaine-activated nucleus accumbens neurons prevents context-specific sensitization. Nat Neurosci *12*, 1069-1073.

Lakatos, P., Shah, A.S., Knuth, K.H., Ulbert, I., Karmos, G., and Schroeder, C.E. (2005). An oscillatory hierarchy controlling neuronal excitability and stimulus processing in the auditory cortex. J Neurophysiol *94*, 1904-1911.

Lim, M.M., Wang, Z., Olazabal, D.E., Ren, X., Terwilliger, E.F., and Young, L.J. (2004). Enhanced partner preference in a promiscuous species by manipulating the expression of a single gene. Nature *429*, 754-757.

Liu, X., Ramirez, S., Pang, P.T., Puryear, C.B., Govindarajan, A., Deisseroth, K., and Tonegawa, S. (2012). Optogenetic stimulation of a hippocampal engram activates fear memory recall. Nature *484*, 381-385.

Mattson, B.J., Koya, E., Simmons, D.E., Mitchell, T.B., Berkow, A., Crombag, H.S., and Hope, B.T. (2008). Context-specific sensitization of cocaine-induced locomotor activity and associated neuronal ensembles in rat nucleus accumbens. Eur J Neurosci *27*, 202-212.

McGraw, L.A., and Young, L.J. (2010). The prairie vole: an emerging model organism for understanding the social brain. Trends Neurosci *33*, 103-109.

Meredith, G.E., Agolia, R., Arts, M.P.M., Groenewegen, H.J., and Zahm, D.S. (1992). Morphological differences between projection neurons of the core and shell in the nucleus accumbens of the rat. Neuroscience *50*, 149-162.

Mitra, P., and Bokil, H. (2008). Observed Brain Dynamics (New York: Oxford University Press).

Mitra, P.P., and Pesaran, B. (1999). Analysis of dynamic brain imaging data. Biophys J *76*, 691-708.

NAMHC (2004). Setting priorities for basic brain & behavioral science research at NIMH: report of the national advisory mental health council's workgroup on basic sciences. U.S. Dept. of Health and Human Services and National Institute of Mental Health.

Nicola, S.M. (2007). The nucleus accumbens as part of a basal ganglia action selection circuit. Psychopharmacology *191*, 521-550.

Nicola, S.M., Surmeier, D.J., and Malenka, R.C. (2000). Dopaminergic modulation of neuronal excitability in the striatum and nucleus accumbens. Annu Rev Neurosci *23*, 185-215.

Nyuyki, K.D., Waldherr, M., Baeuml, S., and Neumann, I.D. (2011). Yes, I am ready now: differential effects of paced versus unpaced mating on anxiety and central oxytocin release in female rats. PLoS ONE *6*, e23599.

Okuyama, T., Kitamura, T., Roy, D.S., Itohara, S., and Tonegawa, S. (2016). Ventral CA1 neurons store social memory. Science *353*, 1536.

Olazábal, D.E., and Young, L.J. (2006). Oxytocin receptors in the nucleus accumbens facilitate “spontaneous” maternal behavior in adult female prairie voles. Neuroscience *141*, 559-568.

Paxinos, G., and Watson, C. (2009). The Rat Brain in Stereotaxic Coordinates, Compact 6th edn (London: Academic Press).

Pennartz, C.M.A., Groenewegen, H.J., and Lopes da Silva, F.H. (1994). The nucleus accumbens as a complex of functionally distinct neuronal ensembles: an integration of behavioural, electrophysiological and anatomical data. Prog Neurobiol *42*, 719-761.

Pfaus, J.G., Damsma, G., Wenkstern, D., and Fibiger, H.C. (1995). Sexual activity increases dopamine transmission in the nucleus accumbens and striatum of female rats. Brain Res *693*, 21-30.

Phillipson, O.T., and Griffiths, A.C. (1985). The topographic order of inputs to nucleus accumbens in the rat. Neuroscience *16*, 275-296.

Ragozzino, M.E., Detrick, S., and Kesner, R.P. (1999). Involvement of the prelimbic-infralimbic areas of the rodent prefrontal cortex in behavioral flexibility for place and response learning. J Neurosci *19*, 4585-4594.

Ross, H.E., Cole, C.D., Smith, Y., Neumann, I.D., Landgraf, R., Murphy, A.Z., and Young, L.J. (2009a). Characterization of the oxytocin system regulating affiliative behavior in female prairie voles. Neuroscience *162*, 892-903.

Ross, H.E., Freeman, S.M., Spiegel, L.L., Ren, X., Terwilliger, E.F., and Young, L.J. (2009b). Variation in oxytocin receptor density in the nucleus accumbens has differential effects on affiliative behaviors in monogamous and polygamous voles. J Neurosci *29*, 1312-1318.

Ryan, S.J., Ehrlich, D.E., Jasnow, A.M., Daftary, S., Madsen, T.E., and Rainnie, D.G. (2012). Spike-timing precision and neuronal synchrony are enhanced by an interaction between synaptic inhibition and membrane oscillations in the amygdala. PLoS ONE *7*, e35320.

Schultz, W. (2006). Behavioral theories and the neurophysiology of reward. Annu Rev Psychol *57*, 87-115.

Slepian, D., and Pollack, H.O. (1961). Prolate spheroidal wave functions, Fourier analysis and uncertainty - I. Bell Syst Tech J *40*, 43-63.

Smith, K.S., Tindell, A.J., Aldridge, J.W., and Berridge, K.C. (2009). Ventral pallidum roles in reward and motivation. Behav Brain Res *196*, 155-167.

Stuber, G.D., Sparta, D.R., Stamatakis, A.M., van Leeuwen, W.A., Hardjoprajitno, J.E., Cho, S., Tye, K.M., Kempadoo, K.A., Zhang, F., Deisseroth, K*., et al.* (2011). Excitatory transmission from the amygdala to nucleus accumbens facilitates reward seeking. Nature *475*, 377-380.

Swanson, L.W. (1982). The projections of the ventral tegmental area and adjacent regions: a combined fluorescent retrograde tracer and immunofluorescence study in the rat. Brain Res Bull *9*, 321-353.

Taverna, S., Canciani, B., and Pennartz, C.M.A. (2007). Membrane properties and synaptic connectivity of fast-spiking interneurons in rat ventral striatum. Brain Res *1152*, 49-56.

Taverna, S., van Dongen, Y.C., Groenewegen, H.J., and Pennartz, C.M.A. (2004). Direct physiological evidence for synaptic connectivity between medium-sized spiny neurons in rat nucleus accumbens in situ. J Neurophysiol *91*, 1111-1121.

Tepper, J.M., Wilson, C.J., and Koós, T. (2008). Feedforward and feedback inhibition in neostriatal GABAergic spiny neurons. Brain Res Rev *58*, 272-281.

Tort, A.B., Komorowski, R., Eichenbaum, H., and Kopell, N. (2010). Measuring phase-amplitude coupling between neuronal oscillations of different frequencies. J Neurophysiol *104*, 1195-1210.

Tort, A.B., Kramer, M.A., Thorn, C., Gibson, D.J., Kubota, Y., Graybiel, A.M., and Kopell, N.J. (2008). Dynamic cross-frequency couplings of local field potential oscillations in rat striatum and hippocampus during performance of a T-maze task. Proc Natl Acad Sci USA *105*, 20517-20522.

van der Meer, M.A., and Redish, A.D. (2009). Low and high gamma oscillations in rat ventral striatum have distinct relationships to behavior, reward, and spiking activity on a learned spatial decision task. Front Integr Neurosci *3*, 9.

van Eden, C.G., and Uylings, H.B.M. (1985). Cytoarchitectonic development of the prefrontal cortex in the rat. J Comp Neurol *241*, 253-267.

van Huijstee, A.N., and Mansvelder, H.D. (2015). Glutamatergic synaptic plasticity in the mesocorticolimbic system in addiction. Front Cell Neurosci 8, 466.

Vertes, R.P. (2004). Differential projections of the infralimbic and prelimbic cortex in the rat. Synapse *51*, 32-58.

Waldherr, M., and Neumann, I.D. (2007). Centrally released oxytocin mediates mating-induced anxiolysis in male rats. Proc Natl Acad Sci U S A *104*, 16681-16684.

Walton, M.E., Bannerman, D.M., and Rushworth, M.F.S. (2002). The role of rat medial frontal cortex in effort-based decision making. J Neurosci *22*, 10996-11003.

Wang, Z., Yu, G., Cascio, C., Liu, Y., Gingrich, B., and Insel, T.R. (1999). Dopamine D2 receptor-mediated regulation of partner preferences in female prairie voles (Microtus ochrogaster): a mechanism for pair bonding? Behav Neurosci *113*, 602-611.

Williams, J.R., Catania, K.C., and Carter, C.S. (1992). Development of partner preference in female prairie voles: the role of social and sexual experience. Horm Behav *26*, 339-349.

Williams, J.R., Insel, T.R., Harbaugh, C.R., and Carter, C.S. (1994). Oxytocin administered centrally facilitates formation of a partner preference in female prairie voles (Microtus ochrogaster). J Neuroendocrinol *6*, 247-250.

Yizhar, O., Fenno, L.E., Prigge, M., Schneider, F., Davidson, T.J., O'Shea, D.J., Sohal, V.S., Goshen, I., Finkelstein, J., Paz, J.T.*, et al.* (2011). Neocortical excitation/inhibition balance in information processing and social dysfunction. Nature *477*, 171-178.

Young, L.J., Lim, M.M., Gingrich, B., and Insel, T.R. (2001). Cellular mechanisms of social attachment. Horm Behav *40*, 133-138.

Young, L.J., and Wang, Z. (2004). The neurobiology of pair bonding. Nature Neurosci *7*, 1048-1054.

Zayas, V., Günaydin, G., and Shoda, Y. (2015). From an Unknown Other to an Attachment Figure: How Do Mental Representations Change as Attachments Form? In Bases of Adult Attachment: Linking Brain, Mind and Behavior, V. Zayas, and C. Hazan, eds. (New York: Springer).

VITA

Elizabeth A. Amadei was born and raised in Boulder, Colorado. She received a B.S. in Engineering Science from Smith College in 2010, where she was awarded the Adeline Devor Penberthy Prize in Engineering. She has pursued doctoral studies as a Georgia Institute of Technology President's Fellow under the directorship of Dr. Robert Liu and Dr. Larry Young.